

Processing of pain and itch information by modality-specific neurons within the anterior cingulate cortex in mice

Received: 31 October 2023

Accepted: 10 February 2025

Published online: 04 March 2025

 Check for updates

Hyung-Gon Ko^{1,2}✉, Hyunsu Jung^{3,4,9}, Seunghyo Han^{1,9}, Dong Il Choi^{4,9}, Chiwoo Lee^{4,9}, Ja Eun Choi⁴, Jihae Oh⁴, Chuljung Kwak³, Dae Hee Han³, Jun-Nyeong Kim¹, Sanghyun Ye⁴, Jiah Lee⁴, Jaehyun Lee⁴, Kyungmin Lee⁵, Jae-Hyung Lee⁶, Min Zhuo^{7,8} & Bong-Kiun Kaang^{3,4}✉

Pain and itch are aversive sensations with distinct qualities, processed in overlapping pathways and brain regions, including the anterior cingulate cortex (ACC), which is critical for their affective dimensions. However, the cellular mechanisms underlying their processing in the ACC remain unclear. Here, we identify modality-specific neuronal populations in layer II/III of the ACC in mice involved in pain and itch processing. Using a synapse labeling tool, we show that pain- and itch-related neurons selectively receive synaptic inputs from mediodorsal thalamic neurons activated by pain and itch stimuli, respectively. Chemogenetic inhibition of these neurons reduced pruriception or nociception without affecting the opposite modality. Conversely, activation of these neurons did not enhance stimulus-specific responses but commonly increased freezing-like behavior. These findings reveal that the processing of itch and pain information in the ACC involves activity-dependent and modality-specific neuronal populations, and that pain and itch are processed by functionally distinct ACC neuronal subsets.

The processing of external stimuli by both the central and peripheral nervous systems promotes the survival of the organism. In the brain, some regions are specifically activated by stimuli with either positive or negative emotional valence, while other regions are activated by stimuli of both types¹. The anterior cingulate cortex (ACC) appears to be heterogeneous, having been implicated in many physiological functions from basic sensation to higher cognition^{2–10}. Although numerous studies have focused on the neurophysiological functions of the ACC individually, how the limited number of ACC neurons can

participate in such breadth of function remains unclear. Is each individual neuron inherently bound to a single specific function? Alternatively, does each ACC neuron perform a specific function as part of a population unit without having its own individual innate function?¹¹ Although neurons activated by negative feelings, pain, sexual attraction, pleasure, and cognition seem to be intermingled in the ACC rather than being separated into specific ACC subregions^{12–14}, we still lack sufficient information about the functional identity of individual neurons to clarify this point.

¹Department of Anatomy and Neurobiology, School of Dentistry, Brain Science and Engineering Institute, Kyungpook National University, 2177 Dalgubeol-daero, Daegu, South Korea. ²Department of Oral Anatomy and Developmental Biology, Kyung Hee University College of Dentistry, Seoul, South Korea. ³Center for Cognition and Sociality, Institute for Basic Science (IBS), Daejeon 34126, South Korea. ⁴Department of Biological Sciences, College of Natural Sciences, Seoul National University, 1 Gwanangno, Seoul, South Korea. ⁵Laboratory for Behavioral Neural Circuitry and Physiology, Department of Anatomy, Brain Science and Engineering Institute, School of Medicine, Kyungpook National University, 680 Gukchaebosang-ro, Daegu, South Korea. ⁶Department of Oral Microbiology, College of Dentistry, Kyung Hee University, 26 Kyungheedaero, Seoul, South Korea. ⁷Department of Physiology, Faculty of Medicine, University of Toronto, 1 King's College Circle, Toronto, Ontario, Canada. ⁸International Institute for Brain Research, Qingdao International Academician Park, Qingdao, China. ⁹These authors contributed equally: Hyunsu Jung, Seunghyo Han, Dong Il Choi, Chiwoo Lee. ✉e-mail: hgko@khu.ac.kr; kaang@ibs.re.kr

One of the functions of the ACC is the cortical processing of pain and itch. Both pain and itch evoke aversive feelings, but the experience of each is qualitatively different. Studies at the spinal level uncovered the transmission of nociceptive and pruriceptive stimuli^{15–17} via primary sensory neurons that respond to both algogens and pruritogens. Although our understanding remains incomplete, sensory receptors expressed on peripheral axon terminals are thought to determine the nociceptive or pruriceptive functionality of these primary sensory neurons¹⁸. These neurons were also shown, however, to transmit the same pain- or itch-specific signal regardless of the type of sensory receptor they express, indicating that they act as labeled lines^{19,20}. Pain and itch signals are transmitted from the spinal cord to the thalamus through the spinothalamic tract (STT) as well as parabrachial nucleus (PBN) and then to several brain regions including the ACC^{21,22}. Although pain and itch signals are known to pass through shared supraspinal neural circuits, it remains unclear how the brain discriminates these two types of signals.

Here, we show how the related but distinct sensations of pain and itch are processed in the ACC. Neurons in the ACC respond to painful and itchy stimuli in two distinct ways. One population of neurons is activated by both stimuli presented within a short time interval, irrespective of the stimulus types. Another population is modality-specific, responding exclusively to specific stimuli. These modality-specific neurons are synaptically connected to presynaptic MD neurons responding to the same modality and contribute to processing corresponding stimuli.

Results

ACC neurons are activated by painful and itchy stimuli in a non-somatotopic manner

While the requirement for the ACC in pain processing has been well-demonstrated, there are few direct lines of evidence implicating the ACC in itch processing²³. Thus, we first confirmed that the ACC is required for detecting both itchy and painful sensations. We used a mixture of the competitive AMPA/kainate receptor antagonist CNQX and the voltage-gated Na⁺ channel blocker TTX to suppress neuronal activity in the ACC. Bilateral microinjection of CNQX + TTX into the ACC reduced scratching behavior induced by injection of the pruritogen histamine, as well as the nociceptive response induced by injection of the algogen formalin (Fig. 1a–c). Next, we tried to identify the ACC neuronal subsets activated by pain or itch stimuli. As a prerequisite, we first verified the pruritogenic and algogenic purity of histamine and formalin, respectively. Histamine injections into the nape of the neck mainly induced antipruriceptive responses such as scratching, rarely inducing antinociceptive responses such as wiping with the forepaw (Fig. 1d). Rather than inducing antipruriceptive responses such as biting, formalin injections into the hindpaw induced antinociceptive responses such as licking, shaking, and lifting (Fig. 1e). In addition, we confirmed literature reports that the ACC does not show somatotopy²⁴. In our previous study, we showed enhancement of fos (+) cells in the ACC induced by harmful stimuli^{25,26}. When we injected either histamine into the nape of the neck or formalin into the hind paw, we observed enhancement of fos (+) cells throughout the ACC without concentrations in specific subregions (Fig. 1f). Additionally, most of these fos (+) cells were co-immunostained with CaMKII, an excitatory neuronal marker rather than GABA, an inhibitory neuronal marker (Fig. 1g–j).

ACC neurons are activated by painful and itchy stimuli in modality-specific or excitability-based manner

Next, we used TetTag (Fos-tTA × tetO-H2BGFP) mice to identify the ACC neuronal subsets activated by pain or itch stimuli. These mice allowed us to label neurons activated by the two stimuli delivered either 6 hours or 3 days apart. We used two distinct time intervals between stimulations because excitability can affect a neuron's

responsivity to a given stimulus^{27–29}. Indeed, previously activated neurons briefly remain in a state of increased excitability in which they are more easily triggered by subsequent stimulations³⁰. In our present study with TetTag mice, we delivered the first stimulus (histamine) in the absence of doxycycline (Dox) after 7 days of intense handling and habituation procedures to eliminate leaky expression induced by background activity. These induced neurons are activated by histamine-expressed GFP-conjugated histone H2B protein (H2BGFP) under the control of the c-fos promoter (Fig. 2a). H2BGFP has a long half-life and can be used as a stable molecular tag in nonproliferating cells such as neurons³¹. We then gave a second stimulus (either histamine or formalin) in the presence of Dox. Because neuronal activation triggers transient Fos expression, although the neurons activated by the second stimulus began to express Fos protein, the presence of Dox prevented them from expressing H2BGFP (Fig. 2a)³². We then focused on ACC layer II/III, which mainly receives thalamic inputs and shows synaptic potentiation in conditions that induce chronic pain or itch^{9,33}. When we analyzed ACC layer II/III in mice that received histamine followed by a second stimulus of formalin (Histamine → Formalin), we found that the proportion of neurons that responded to both stimuli when they were delivered 6 h apart was higher than would be expected by chance alone. In contrast, the proportion of neurons that responded to both stimuli when they were delivered 3 days apart could be explained by chance alone (Fig. 2b, d and f). Thus, these neurons activated by histamine were preferentially activated by a subsequent formalin injection when the interstimulus interval was 6 h rather than 3 days. In a control experiment, we also confirmed reduced scratching behavior 6 h after the initial histamine injection (Supplementary Fig. 1). This allowed us to eliminate the possibility that the effect of the first stimulus (histamine) remained through the administration of the second stimulus (formalin). In addition, not only was a similar proportion of neurons activated by formalin injection at 6 h or 3 days after histamine injection, a similar proportion of neurons was activated by histamine at 6 h or 3 days before formalin injection (Supplementary Fig. 2a, b). To determine whether this effect is specific to layer II/III of the ACC, we extended our analysis to all layers of the ACC combined. When we did so, we did not find the same pattern of neuronal activation we observed in layer II/III (Supplementary Fig. 3). Nor did we observe a similar neuronal activation pattern in layer II/III of the retrosplenial cortex, which is located directly posterior to the ACC (Supplementary Fig. 4). Thus, there exists a neuronal subset within the ACC that is activated by both algogenic and pruritogenic stimuli administered within a short time of one another. This activated pattern seems to be an intrinsic feature of neurons located in ACC layer II/III. Next, we analyzed ACC layer II/III neurons in TetTag mice injected with histamine as both the first and second stimuli (Histamine → Histamine). Interestingly, regardless of the time interval between the stimuli (i.e., 6 h or 3 days), the proportion of neurons responding to both stimuli was both similar and higher than that expected due to chance alone (Fig. 2c, e and f). As in the Histamine → Formalin experiment, H2BGFP and Fos expression were similar in the 6-h and 3-day interval groups (Supplementary Fig. 2c and d). These results indicate that a subset of ACC neurons show modality-specific activation, regardless of the timing of their last activation. When the two stimuli are given at a sufficient time interval (3 days) to exclude the effect of excitability, Itch → Itch shows a higher reactivation index than Itch → Pain, further supporting the existence of modality-specific neurons (Fig. 2f).

Modality-specific or excitability-based activation of ACC neurons by painful and itchy stimuli in freely moving mice

To investigate this neuronal activation pattern more precisely, we chose to use a miniscope, which is a head-mounted miniature fluorescent microscope. This allowed us to observe ACC neuron activation

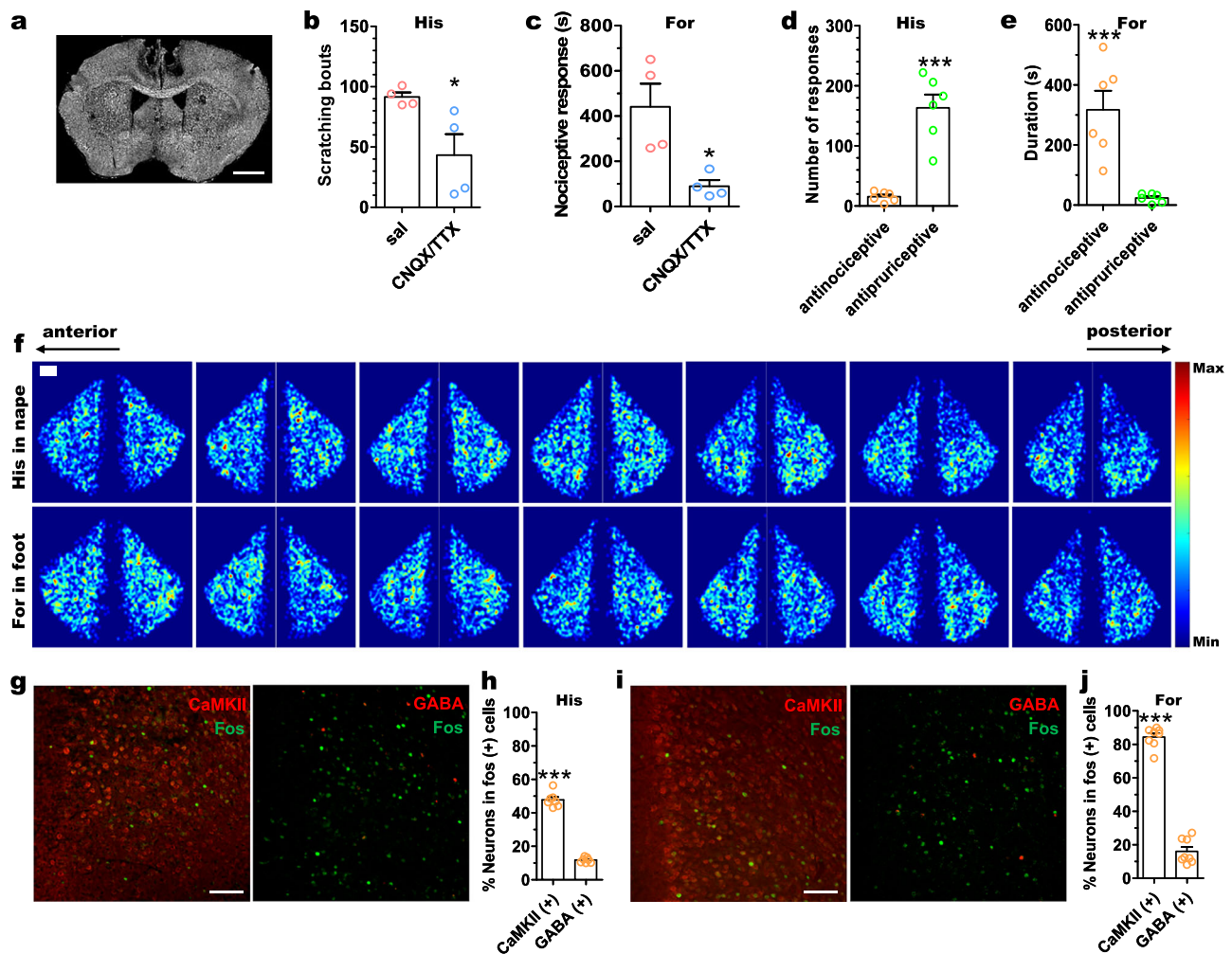


Fig. 1 | ACC neurons are required for pain and itch responses without showing somatopy. **a** Representative image showing microinjection site in the ACC. Scale bar, 1 mm. **b** Scratching behavior after histamine injection ($n = 4$ mice in sal, $n = 4$ mice in CNQX/TTX; two-tailed unpaired t-test, $t_6 = 2.704$, $*p = 0.0354$). **c** Nociceptive behavior after formalin injection ($n = 4$ mice in sal, $n = 4$ mice in CNQX/TTX; two-tailed unpaired t-test, $t_6 = 3.338$, $*p = 0.0157$). **d, e** Antinociceptive and antiprurceptive responses induced by histamine injection in the nape of the neck (**d** $n = 6$ mice in measuring antinociceptive and antiprurceptive responses; two-tailed unpaired t-test, $t_{10} = 6.565$, $***p < 0.0001$) or formalin injection in the left hind sole (**e** $n = 6$ mice in measuring antinociceptive and antiprurceptive responses; two-tailed unpaired t-test, $t_{10} = 4.610$, $***p = 0.0010$). **f** The distribution of fos (+) cells in the whole ACC. Six mice per group were injected with histamine in the

nape of the neck or formalin in the left hind sole. The distribution of fos (+) cells reconstructed in heatmaps. Scale bars, 200 μm . **g** Representative double immunolabeling images of the ACC showing CaMKII and Fos (left), and GABA and Fos (right) in histamine-injected mice. Scale bars, 100 μm . **h** Percentage of cells co-stained with CaMKII or GABA among total fos (+) cells ($n = 7$ mice injected with His; two-tailed unpaired t-test, $t_{12} = 20.32$, $***p < 0.0001$). **i** Representative double immunolabeling images of the ACC showing CaMKII and Fos (left), and GABA and Fos (right) in formalin-injected mice. Scale bars, 100 μm . **j** Percentage of cells co-stained with CaMKII or GABA among total fos (+) cells ($n = 8$ mice injected with For; two-tailed unpaired t-test, $t_{14} = 20.20$, $***p < 0.0001$). sal Saline, His Histamine, For Formalin. Data presented as mean \pm SEM. Source data are provided as a Source Data file.

in response to sensory stimuli in real time on freely moving mice (Fig. 3a)³⁴. First, we asked how ACC neurons responding to the two stimuli varied according to the time interval. After 7 days of handling and habituation, we gave two stimuli (histamine or formalin) with either a 6-h or 3-day interval between them. Neurons were divided into three groups: those that fired before and after stimulus injection, those that fired only before stimulus injection, and those that fired only after stimulus injection (Fig. 3b, c). We only included the last group (referred to as only after neurons) in our calculation of the percentage of neurons with overlapping response profiles because the former two groups likely contained neurons activated by background stimuli. The percentage of overlapping neurons that responded to both histamine and formalin stimulation was significantly higher for stimulations given at a 6-h interval than for those given at a 3-day interval (Fig. 3d, e). When we gave two consecutive histamine injections within a 6-h or 3-day interval, we found no significant difference in the overlapping

population between the two groups (Fig. 3f, g). These results were consistent with our immunohistological analysis of the TetTag mice (Fig. 2). As a negative control, we analyzed neurons that fired only before (referred to as only before neurons) and both before and after (referred to as both before and after neurons) stimulus injection. First, only before neurons were considered to represent those responding to the experimental context but unrelated to the stimulus itself. They showed higher reactivation when the two stimuli were given at a 6-h interval compared to a 3-day interval (Supplementary Fig. 5a–c). This result suggests that once neurons specifically responding to the experimental context are activated, they maintain high excitability for a certain period. Next, we analyzed both before and after neurons, which were assumed to exhibit spontaneous activity. This class of neurons did not show any difference in reactivation between the groups (Supplementary Fig. 5d–f). In contrast to the analysis of stimulus-specific only after neurons, the analysis including both before

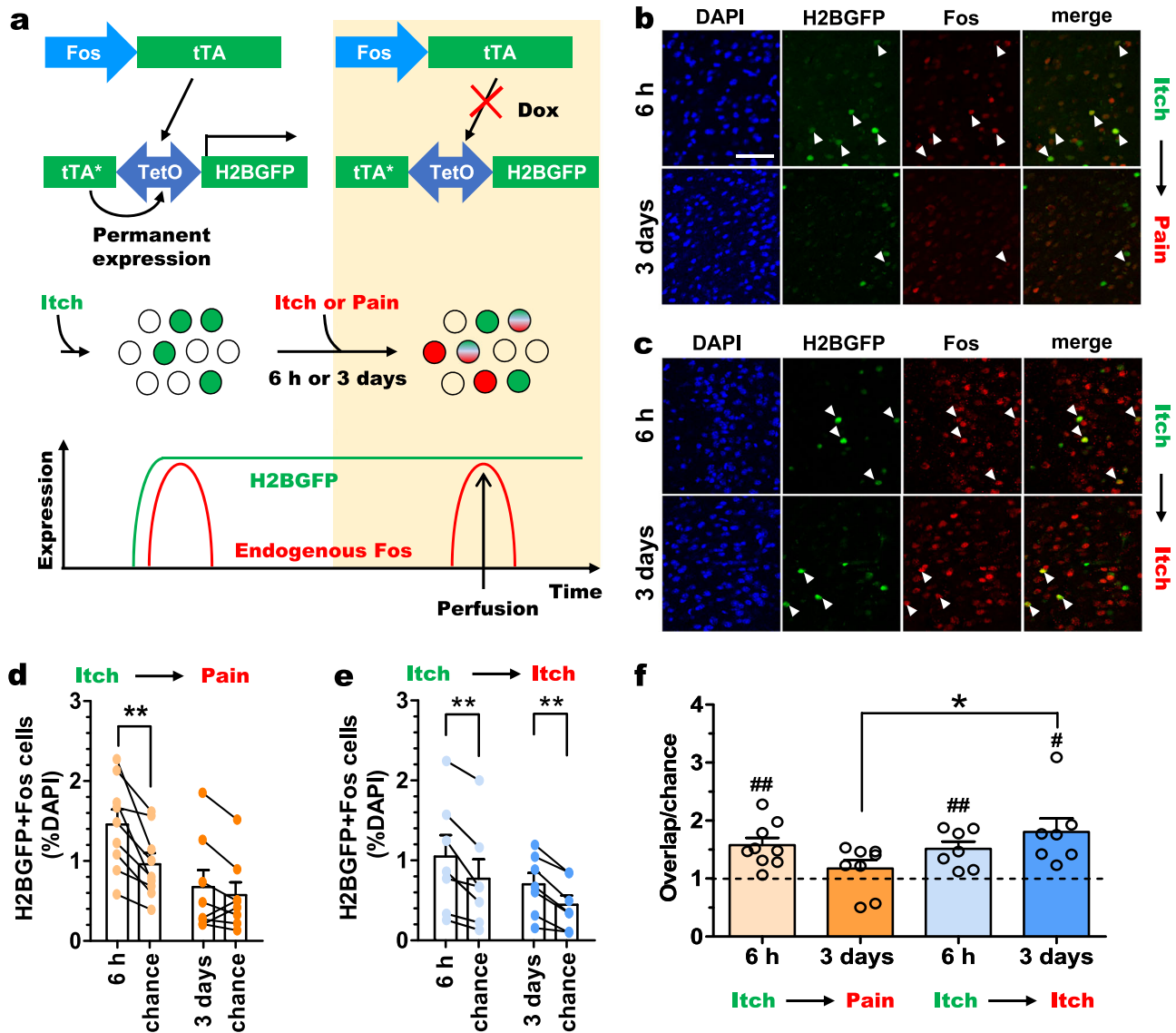


Fig. 2 | Labeling of neurons activated by pruritogenic and algogenic stimuli over a time interval. **a** Experimental scheme. **b, c** Representative immunolabeling images of the ACC in mice that waited 6 h or 3 days between histamine and formalin stimuli (**b**) or between histamine and histamine stimuli (**c**). White arrowheads indicate H2BGFP and Fos double (+) cells. Scale bars, 50 μm. **d** The proportion of neurons activated by both itch- and pain-inducing stimuli, given either with a 6-h or a 3-day interval ($n = 9$ mice in 6-h interval, $n = 8$ mice in 3-day interval; two-tailed paired t-test; 6-h interval, $t_8 = 4.301$, ** $p = 0.0026$; 3-day interval, $t_7 = 1.247$, $p = 0.2524$). **e** The proportion of neurons activated by both consecutive itch-inducing stimuli, given with a 6-h or 3-day interval ($n = 7$ mice in 6-h interval, $n = 7$ mice in 3-day interval; two-tailed unpaired t-test; 6-h interval, $t_6 = 4.008$,

** $p = 0.0071$; 3-day interval, $t_6 = 5.860$, ** $p = 0.0011$). **f** Levels of reactivation index (overlap/chance) were above chance except for Itch → Pain at the 3-day interval ($n = 9$ mice in Itch → Pain 6-h interval, $n = 8$ mice in Itch → Pain 3-day interval, $n = 7$ mice in Itch → Itch 6-h interval, $n = 7$ mice in Itch → Itch 3-day interval; one sample t-test, chance = 1; Itch → Pain at the 6-h interval, $t_8 = 4.568$, ## $p = 0.0018$; Itch → Pain at the 3-day interval, $t_7 = 1.207$, $p = 0.2666$; Itch → Itch at the 6-h interval, $t_6 = 4.173$, ## $p = 0.0059$; Itch → Itch at the 3-day interval, $t_6 = 3.440$, # $p = 0.0138$). The overlap/chance at the 3-day interval was higher in the Itch → Itch group compared to Itch → Pain group (two-tailed unpaired t-test; $t_{13} = 2.356$, * $p = 0.0349$). The dotted line indicates chance level. Data presented as mean ± SEM. Source data are provided as a Source Data file.

and after neurons did not reveal a higher reactivation rate when histamine and formalin were administered at the 6-h interval compared to the 3-day interval (Supplementary Fig. 5g-i).

Next, we asked whether itch- and pain-specific neuronal populations in the ACC have any inherent properties that distinguish them from one another. The mean firing frequency distribution showed a significant difference between neurons that fired only before and those that fired only after the stimulus (either histamine or formalin) (Supplementary Fig. 6a-d). Moreover, itch- and pain-specific neuronal populations showed a significant difference in mean firing frequency (Supplementary Fig. 6e). Additionally, when we used a machine learning algorithm to classify these activated neurons, we found that

the neuronal firing patterns were clearly distinguishable according to stimulus. (Fig. 3h, Supplementary Fig. 7, and Supplementary Table. 1). These results support the existence of modality-specific neurons in the ACC.

Pain- or itch-specific ACC neurons receive modality-specific presynaptic inputs from the mediodorsal thalamus (MD)

The ACC receives presynaptic inputs from multiple brain regions. We, therefore, asked whether pain- or itch-specific neurons in the ACC are specifically connected to presynaptic neurons activated by identical stimuli. The MD acts as a presynaptic region upstream of the ACC in the processing of the affective dimension of pain³⁵. When

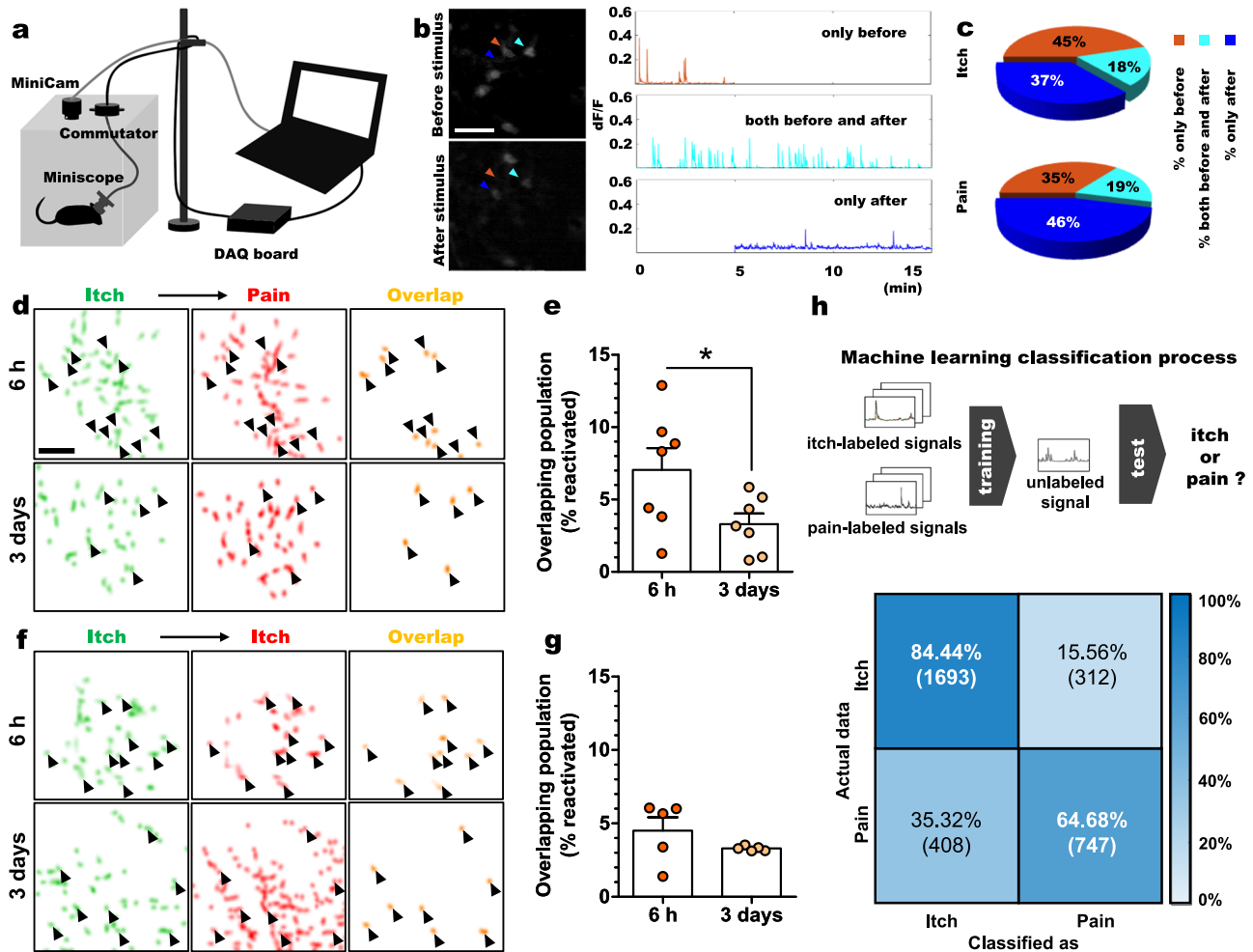


Fig. 3 | In vivo imaging of pain and itch-responsive populations. **a** Schematic for the miniscope recordings. **b** Representative images captured via miniscope before (upper) and after (lower) stimulus injection. Brown arrowhead indicates neurons activated only before stimulus. Cyan arrowhead indicates neuron activated both before and after the stimulus. The blue arrowhead indicates neurons activated only after the stimulus. Calcium imaging traces of the neurons marked with arrowheads are shown in matching colors on the right. Scale bar, 100 μ m. **c** Proportion of neurons activated only before, both before and after, and only after histamine or formalin injection. **d** Representative rendering images of neurons activated only after stimulus. Neurons activated by itch-inducing or pain-inducing stimuli are marked in green or red, respectively. Neurons activated by both stimuli at 6-h or 3-day intervals are marked in orange. Black arrowheads indicate neurons activated by both stimuli at 6-h or 3-day intervals. Scale bar, 100 μ m. **e** Percentage of overlapping neurons responding to histamine and formalin given at 6-h or 3-day

intervals ($n = 7$ mice in 6-h interval, $n = 7$ mice in 3-day intervals; two-tailed unpaired t -test, $t_{12} = 2.219$, $*p = 0.0465$). **f** Representative images of neurons activated only after stimulus injection. Neurons activated by the first or second itch-inducing stimulus are marked with green or red, respectively. Neurons activated by both stimuli at 6-h or 3-day intervals are marked in orange. Black arrowheads indicate neurons activated by both stimuli at 6-h or 3-day intervals. Scale bar, 100 μ m. **g** Percentage of overlapping neurons responding to two consecutive histamine injections given at 6-h or 3-day intervals ($n = 5$ mice in 6-h intervals, $n = 5$ mice in 3-day intervals; two-tailed paired t -test, $t_4 = 1.267$, $p = 0.2738$). **h** Machine learning classification of neurons activated only after stimulation (histamine or formalin) (above: overview, below: confusion matrix). The top-left or bottom-right quadrants: the percentage (number) of correctly classified neurons. The top-right or bottom-left quadrants: the percentage (number) of incorrectly classified neurons. Data presented as mean \pm SEM. Source data are provided as a Source Data file.

we injected monosynaptic retrograde canine adenovirus expressing *Cre* (CAV-cre) into the ACC of *Ai14* mice, we observed tdTomato-labeled somata in several thalamic subnuclei, including the MD (Supplementary Fig. 8). Consistent with a previous study, we found that the ACC receives inputs mainly from the lateral MD^{35,36}. Next, we tested synaptic connectivity between modality-specific neurons in the ACC and the MD using dual-eGRASP (enhanced green fluorescent protein reconstitution across synaptic partners)^{37,38}. To identify neurons activated by both kinds of stimuli, we used an AAV-driven TetTag system in TRAP2 mice. By stimulating TRAP2 mice injected in the ACC and MD with 3 kinds of AAVs (EF1 α -DIO-mCherry, Fos-rtTA, and TRE3G-mEmeraldNuc), we found that neurons activated by histamine or formalin expressed mCherry or mEmeraldNuc, respectively (Supplementary Fig. 9a, b). We were again able to confirm the

presence of separate neuronal populations in the ACC activated by itch or pain stimuli, but we also found this activation pattern in the MD (Supplementary Fig. 9c, d). Based on these results, we used the dual-eGRASP system to examine the connectivity of the ACC and MD at the synapse level. We expressed the GFP variant protein's two components in pre- (MD) and postsynaptic neurons (ACC) under the control of the *c-fos* promoter. When the two components were reconstituted across a synaptic cleft, they appeared as a specific color of fluorescence, either cyan or yellow. In this experiment, we injected several AAV combinations into the ACC (Fos-rtTA, TRE3G-myr_mScarlet-I-P2A-post eGRASP, EF1 α -DIO-myr_iRFP670-P2A-post eGRASP) and MD (Fos-rtTA TRE3G-yellow pre eGRASP, EF1 α -DIO-cyan pre eGRASP) of TRAP2 mice (Fig. 4a and b). In our AAV-based TetTag system, 4-OHT induced iRFP and post-eGRASP in the ACC and

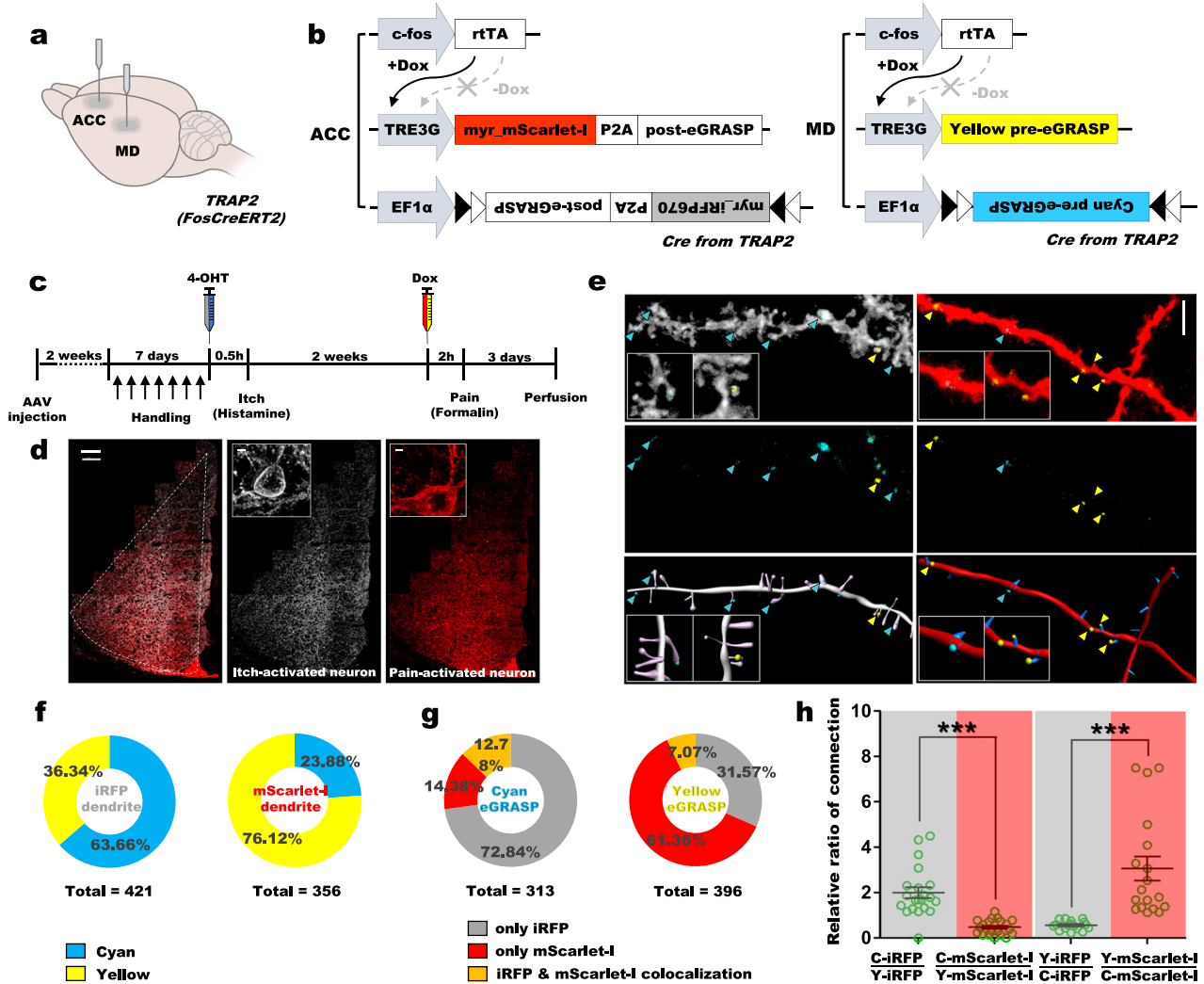


Fig. 4 | Paired synaptic connections between modality-specific neurons in the ACC and MD. **a** Illustration of the viral injection site in a *TRAP2* mouse. **b** Schematic of the AAV constructs and their combinations injected in the MD and ACC. **c** Experimental scheme. **d** Representative images showing virus expression in the ACC among 4 mice used in dual e-GRASP experiments. Expression of iRFP670 indicates itch-activated neurons (middle), while expression of mScarlet-I indicates pain-activated neurons (right). A color-merged image marking the ACC area with a dotted line appears in the left panel. Scale bar, 100 μ m. Inset images showed a magnified itch-activated (middle upper) or pain-activated (right upper) neuron, respectively. Scale bar, 3 μ m. **e** Representative images showing dual eGRASP in itch-activated and pain-activated ACC dendrites with cyan eGRASP puncta (synapses originating from itch-activated MD neurons) and yellow eGRASP puncta (synapses

originating from pain-activated MD neurons). A total of 29 z-stack images were acquired from ACC slices of 4 mice. Above: color-merged raw image. Middle: raw image with only eGRASP signals extracted. Below: 3D reconstruction of dendrites and spines overlaid with eGRASP signals. Cyan and yellow arrowheads indicate cyan and yellow eGRASP puncta, respectively. Scale bar, 4 μ m. **f** The percentage of eGRASP puncta located on iRFP- and mScarlet-I-expressing ACC dendrites. **g** The percentage of iRFP- and mScarlet-I-expressing dendrites located on cyan or yellow eGRASP signals. **h** The relative ratio of these GRASP signals indicates that synaptic inputs to ACC neurons are predetermined by their presynaptic MD neurons ($n = 21$ images of 4 mice in C/Y ratio, $n = 18$ images of 4 mice in Y/C ratio; two-tailed Mann-Whitney U test, $***p < 0.0001$). C Cyan eGRASP puncta, Y Yellow eGRASP puncta. Data presented as mean \pm SEM. Source data are provided as a Source Data file.

cyan pre-eGRASP in the MD upon histamine injection. Under doxycycline, formalin injection induced mScarlet-I and post-eGRASP in the ACC and yellow pre-eGRASP in the MD (Fig. 4c). As a result, neural dendrites activated by histamine or formalin were marked with iRFP or mScarlet-I, respectively. The resulting cyan and yellow eGRASP puncta represent synaptic connections with itch- and pain-activated MD presynaptic inputs, respectively. Consistent with our previous results using TetTag mice and miniscope imaging, we observed ACC neurons activated by histamine and formalin stimuli (Fig. 4d). When we analyzed the eGRASP puncta in dendrites activated by itch or pain-inducing stimuli, we found more cyan eGRASP puncta from itch-activated MD neurons located on iRFP-expressing dendrites of ACC neurons activated by itch-inducing stimuli (Fig. 4e, f; on iRFP-expressing dendrites: yellow eGRASP = 36.34%,

cyan eGRASP = 63.66%). Moreover, we observed more yellow eGRASP puncta from pain-activated MD neurons located on mScarlet-I-expressing dendrites of ACC neurons activated by pain-inducing stimuli (Fig. 4e, f; on mScarlet-I-expressing dendrites: yellow eGRASP = 76.12%, cyan eGRASP = 23.88%). These modality-specific connections between the ACC and MD were consistent with our eGRASP puncta-based dendritic analysis (Fig. 4e, g; cyan eGRASP: 72.84% on iRFP-expressing dendrites, 14.38% on mScarlet-I-expressing dendrites, and 12.78% on dendrites co-expressing both; yellow eGRASP: 61.36% on mScarlet-I-expressing dendrites, 31.57% on iRFP-expressing dendrites, and 7.07% on dendrites co-expressing both). These results were not caused by a difference in the expression strength between the TetTag and TRAP2 system because our analysis of the relative ratio of the connections also showed

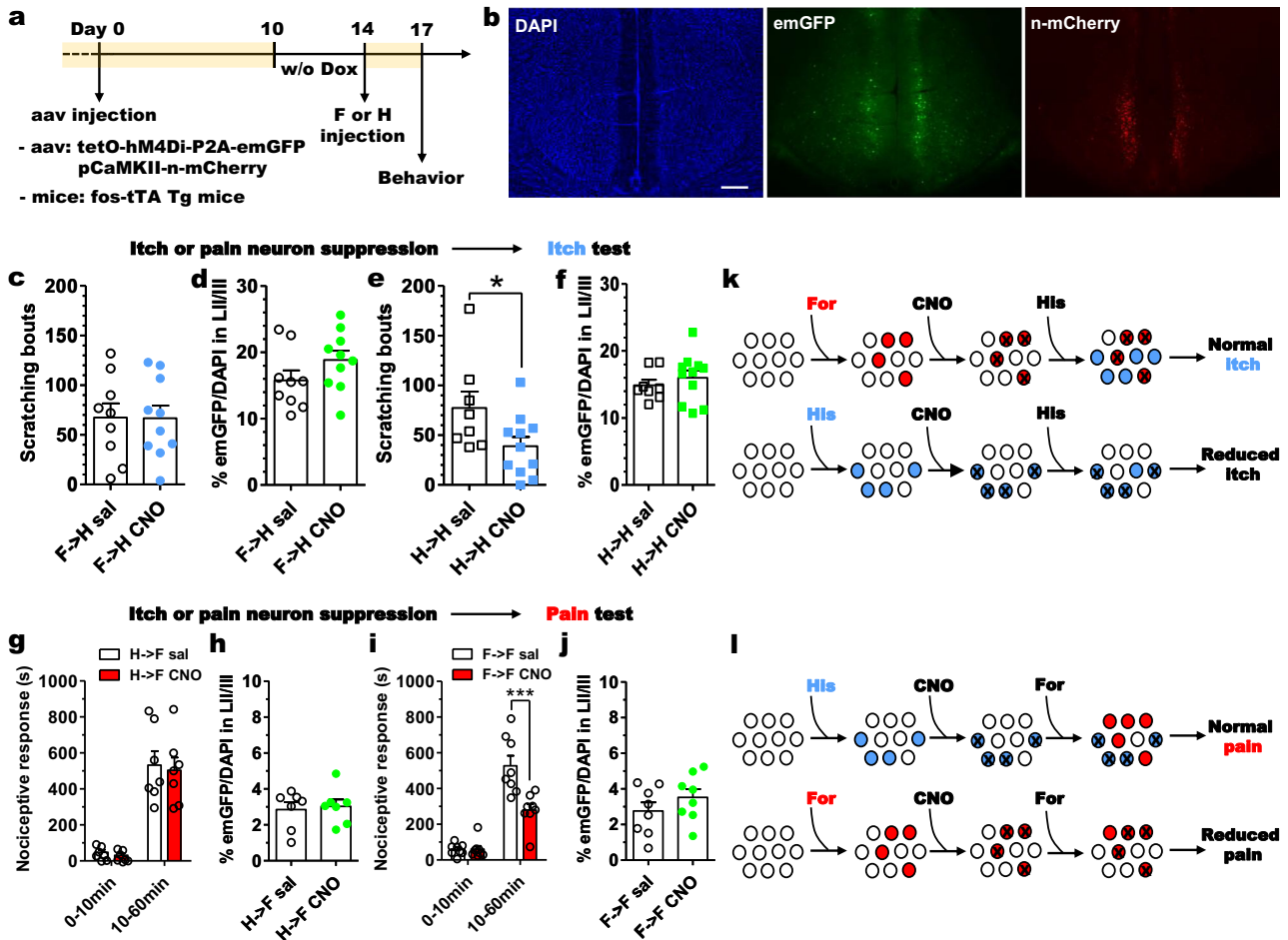


Fig. 5 | Itch- or pain-specific neurons are required for scratching or nociceptive behavior, respectively. **a** Experimental scheme. **b** Representative images of emGFP and n-mCherry expression among the ACC of total of 68 mice. Scale bar, 200 μ m. **c, d** Scratching behavior (**c**) and the proportion of hM4Di-expressing neurons (**d**) ($n = 9$ mice in F \rightarrow H sal, $n = 10$ mice in F \rightarrow H CNO). **c**: two-tailed unpaired t-test, $t_{17} = 0.03335$, $p = 0.9738$. **d** two-tailed unpaired t-test, $t_{17} = 1.491$, $p = 0.1544$. **e, f** Scratching behavior (**e**) and the proportion of hM4Di-expressing neurons (**f**) ($n = 8$ mice in H \rightarrow H sal, $n = 11$ mice in H \rightarrow H CNO). **e**: two-tailed unpaired t-test, $t_{17} = 2.160$, $*p = 0.0454$. **f** two-tailed unpaired t-test, $t_{17} = 0.7668$, $p = 0.4537$. **g, h** Nociceptive responses (**g**) and the proportion of hM4Di-expressing neurons (**h**) ($n = 7$ mice in H \rightarrow F sal, $n = 7$ mice in H \rightarrow F CNO). **g** two-way repeated measures

ANOVA: effect of time, $F_{(1,12)} = 81.58$, $p < 0.0001$; effect of CNO, $F_{(1, 12)} = 0.1758$, $p = 0.6824$; interaction effect, $F_{(1, 12)} = 0.01248$, $p = 0.9129$. **h** two-tailed unpaired t-test, $t_{12} = 0.3180$, $p = 0.7559$. **i, j** Nociceptive responses (**i**) the proportion of hM4Di-expressing neurons (**j**) ($n = 8$ mice in F \rightarrow F sal, $n = 8$ mice in F \rightarrow F CNO). **i** two-way repeated measures ANOVA followed by Bonferroni post-test: effect of time, $F_{(1,14)} = 114.6$, $p < 0.0001$; effect of CNO, $F_{(1, 14)} = 11.42$, $p = 0.0045$; interaction effect, $F_{(1, 14)} = 15.16$, $p = 0.0016$; post-test, $***p < 0.001$. **j** two-tailed unpaired t-test, $t_{14} = 1.148$, $p = 0.2703$. **k, l** Schematic diagram of an itch (**k**) and pain (**l**) on suppression of modality-specific ACC neurons. sal Saline, F Formalin, H Histamine. Data presented as mean \pm SEM. Source data are provided as a Source Data file.

modality-specific connections between the ACC and MD (Fig. 4h). These results indicate the sensory stimuli ACC neurons process are predetermined by their presynaptic MD inputs.

Inhibiting pain-specific ACC neurons only alleviated pain without affecting itch, while inhibiting itch-specific ACC neurons only relieved itch without influencing pain

Finally, we wanted to determine whether modality-specific neurons in the ACC are functionally segregated in the processing of pain and itch modalities. To this end, we used a chemogenetic silencing approach in which we co-injected an AAV expressing the inhibitory designer receptor exclusively activated by designer drugs (DREADD) hM4Di and an AAV expressing mCherry into the ACC of Fos-tTA transgenic mice (Fig. 5a). For the DREADD system, we expressed hM4Di under the tetO promoter so that neurons only express hM4Di (and emGFP) when activated in the absence of Dox (Fig. 5b). After inducing expression of hM4Di in neurons activated in response to an initial algogenic formalin or pruritogenic histamine injection, we inhibited the previously activated neurons 3 days later using clozapine-N-oxide (CNO) and

performed an itch test after another histamine injection. We speculated two possible scenarios. If we observed a suppression of histamine-induced scratching triggered by inhibition of neurons previously activated by formalin, it would indicate that there is no functional segregation of itch- and pain-specific neurons. If, however, we observed a suppression of scratching behavior triggered by inhibiting neurons previously activated by histamine rather than formalin, it would indicate the presence of itch-specific neurons in the ACC. We found that the latter scenario was indeed the case. When we used CNO to inhibit hM4Di-expressing neurons previously activated by formalin injection, we did not observe any change in histamine-induced scratching behavior (Fig. 5c). These results were not caused by reduced expression of hM4Di due to formalin exposure (Fig. 5d). Additionally, the inhibitory effect of CNO on hM4Di-expressing neurons was confirmed through electrophysiological analysis (Supplementary Fig. 10a–c). In contrast, when we inhibited neurons previously activated by histamine, we observed reduced histamine-induced scratching (Fig. 5e, f). Next, when we applied the same experimental scheme using the formalin-induced nociceptive response (pain test) as

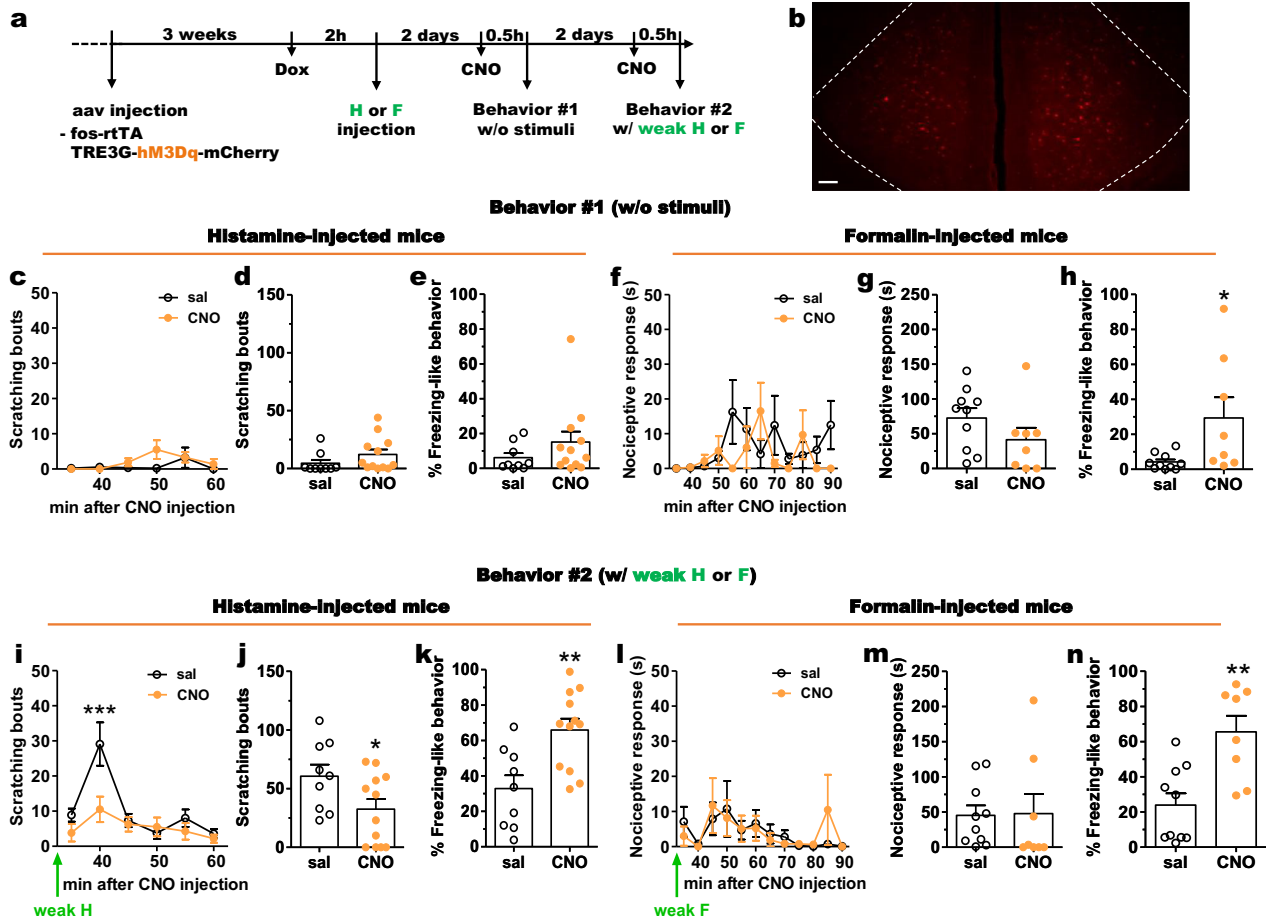


Fig. 6 | Activation of itch- or pain-specific neurons contribute to inducing pruritogen- and algogen-induced anxious states. **a** Experimental scheme. **b** Representative images showing mCherry expression in the ACC of a total of 39 mice. Scale bar, 100 μ m. **c–e** Scratching bouts (**c**, **d**) and freezing-like behavior (**e**) when neurons previously activated by histamine were activated using CNO ($n = 9$ mice in sal, $n = 12$ mice in CNO). **c** two-way repeated measures ANOVA: effect of time, $F_{(5, 95)} = 2.022, p = 0.0825$; effect of CNO, $F_{(1, 95)} = 1.834, p = 0.1915$; interaction effect, $F_{(5, 95)} = 1.277, p = 0.2802$. **d** two-tailed unpaired t-test, $t_{19} = 1.354, p = 0.1915$. **e** two-tailed unpaired t-test, $t_{19} = 1.223, p = 0.2361$. **f–h** Nociceptive responses (**f**, **g**) and freezing-like behavior (**h**) when neurons previously activated by formalin were activated using CNO ($n = 10$ mice in sal, $n = 8$ mice in CNO). **f** two-way repeated measures ANOVA: effect of time, $F_{(11, 176)} = 1.188, p = 0.2986$; effect of CNO, $F_{(1, 176)} = 2.029, p = 0.1736$; interaction effect, $F_{(11, 176)} = 1.533, p = 0.1231$. **g** two-tailed unpaired t-test, $t_{16} = 1.424, p = 0.1736$. **h** two-tailed unpaired t-test, $t_{16} = 2.384, *p = 0.0298$. **i–k** Weak histamine-induced scratching bouts (**i**, **j**) and freezing-like

behavior (**k**) when neurons previously activated by histamine were activated using CNO ($n = 9$ mice in sal, $n = 12$ mice in CNO). **i**: two-way repeated measures ANOVA followed by Bonferroni post-test: effect of time, $F_{(5, 95)} = 11.62, p < 0.0001$; effect of CNO, $F_{(1, 95)} = 4.592, p = 0.0453$; interaction effect, $F_{(5, 95)} = 4.093, p = 0.0021$; post-test, $***p < 0.001$. **j**: two-tailed unpaired t-test, $t_{19} = 2.143, *p = 0.0453$. **k**: two-tailed unpaired t-test, $t_{19} = 3.368, **p = 0.0032$. **l–n**, Weak formalin-induced nociceptive responses (**l**, **m**) freezing-like behavior (**n**) and when neurons previously activated by formalin were activated using CNO ($n = 10$ mice in sal, $n = 8$ mice in CNO). **l** two-way repeated measures ANOVA: effect of time, $F_{(11, 176)} = 1.884, p = 0.0442$; effect of CNO, $F_{(1, 176)} = 0.006581, p = 0.9364$; interaction effect, $F_{(11, 176)} = 0.5102, p = 0.8948$. **m** two-tailed unpaired t-test, $t_{16} = 0.08112, p = 0.9364$. **n** two-tailed unpaired t-test; two-tailed unpaired t-test, $t_{16} = 3.739, **p = 0.0018$. sal Saline, H Histamine, F Formalin. Data presented as mean \pm SEM. Source data are provided as a Source Data file.

the outcome rather than the itch test, we observed the same result as with the itch test. When we inhibited neurons previously activated by histamine, we did not observe any suppression of the nociceptive response induced by formalin (Fig. 5g, h). However, when neurons previously activated by formalin were inhibited, suppression of the nociceptive response to formalin was observed, specifically in the late phase (Fig. 5i, j). These findings indicate that there are modality-specific neuronal subsets in the ACC that process itchy and painful stimuli separately and that cannot functionally substitute for one another (Fig. 5k, l).

Activating pain-specific or itch-specific ACC neurons does not increase pain or itch, but rather heightens the freezing response
 What happens if these itch- or pain-specific neurons are activated? To address this question, gain-of-function experiments were designed using a Fos promoter-based hM3Dq expression system (Fig. 6a). To

selectively express hM3Dq in neurons activated only by pruritogen or algogen, the AAV mixture (Fos-rtTA, TRE3G-hM3Dq-mCherry) was injected into the ACC of wildtype mice (Fig. 6b). Under Dox administration, histamine or formalin was injected, and CNO was used to selectively activate itch- or pain-specific neurons. Electrophysiological recordings showed that hM3Dq-expressing neurons are activated by CNO treatment (Supplementary Fig. 10a, b, and d). First, these specific neuronal populations were activated without any stimuli, revealing no significant changes in scratching bouts when itch-specific neurons were activated or in the nociceptive response when pain-specific neurons were activated (Fig. 6c, d, f, and g). However, body scratching and paw licking are typical grooming behaviors in rodents. These behaviors did not manifest immediately after entering the behavioral chamber but rather after some degree of adaptation (Fig. 6c and f). Therefore, these actions potentially represent grooming behaviors rather than actual anti-pruriceptive or anti-nociceptive responses.

While the activation of itch-specific neurons showed no significant results, a significant increase was observed in freezing-like behavior when pain-specific neurons were activated (Fig. 6e, h). Second, weak histamine-induced scratching bouts and weak formalin-induced nociceptive responses were monitored after activating itch- and pain-specific neurons with CNO, respectively. The scratching bouts significantly decreased rather than increased after CNO injection, with no significant change observed in the nociceptive response (Fig. 6i, j, l, and m). However, the extent to which the reduction in scratching bouts accurately represents a reduction in itchiness remains uncertain. This is due to a significant increase in freezing-like behavior, and this increase was also observed upon activation of pain-specific neurons (Fig. 6k, n). This is not a side effect of CNO because CNO administration did not change freezing-like behavior in Tet-On system-based hM4Di-DREADD experiments (Supplementary Fig. 11e and g). The ACC is the brain region that processes pain and the anxiety associated with it³⁹. Thus, while itch- and pain-specific neuronal populations in the ACC are independent of each other, they induce fear or anxious internal states in responses to corresponding noxious stimuli. Unlike the Tet-Off system using *fos-tTA* transgenic mice in the hM4Di-DREADD experiments (Fig. 5), we employed the Tet-On system using AAVs in this activating hM3Dq-based behavioral experiments. Although we confirmed the hM3Dq/hM4Di receptor expressions and their functionalities in the ACC, we attempted to reproduce hM4Di-based behavioral experiments using the same AAV-based Tet-On system. Additionally, we examined whether inhibiting neurons activated by a specific pruritogen or algogen could suppress itch or pain induced by another pruritogen or algogen, respectively. Consequently, inhibiting neurons previously activated by histamine or formalin respectively decreased scratching bouts or nociceptive responses induced by chloroquine or capsaicin (Supplementary Fig. 11). Collectively, these findings suggest that itch- and pain-specific neuronal populations are distinctly segregated within the ACC, but they commonly induce anxious or fearful states irrespective of the subtype of harmful stimuli.

Discussion

Here, we found that pain and itch information are processed by separate neuronal populations in the ACC. These modality-specific neurons are connected to presynaptic MD neurons activated by stimuli associated with the same modality. We found that the inhibition of pain-specific neurons did not affect itch perception, nor did the inhibition of itch-specific neurons affect pain perception. Many studies have mapped brain neurons activated by various stimuli without confirming the functionality of the labeled neurons. In this study, we showed that the neuronal populations activated by pain and itch stimuli are functionally segregated (Fig. 5). Additionally, these distinct neuronal populations commonly induce negative emotional or anxious internal states regardless of stimulus modality (Fig. 6). Moreover, an additional neuronal population exhibited an activity pattern based on excitability.

An interesting feature of these modality-specific neuronal populations is that, while less than 10% of neurons are activated by two consecutive itch-inducing stimuli, inhibiting neurons previously activated by histamine significantly reduces subsequent histamine-induced itch responses. Additionally, this consistently low overlap was observed between stimuli of different subtypes within the same modality (Supplementary Fig. 12), aligning with findings from a previous study⁴⁰. Thus, we hypothesize that modality-specific neurons are not arranged in a functionally even hierarchy. The ACC may contain a small number of core neurons that handle pain or itch stimuli. Our behavioral findings support the hypothesis that core neurons in the ACC are consistently activated in response to pain or itch stimuli, while the remaining neurons specific to each modality are recruited more variably. Another related hypothesis is that the modality-specific neuronal population in the ACC, driven by population activity and/or

connectivity, induces the anxious or fearful emotional state associated with pain or itch. Recent studies support this view that the activity of neuronal populations, rather than individual neurons, plays a crucial role in processing noxious stimuli^{40–42}.

In addition to modality-specific neurons, we found another class of ACC neuron that responds to stimuli based on the time that has elapsed since a previous stimulation, regardless of stimulus modality. This population was easily activated by two stimuli separated by a short (6-h) interval, but not by stimuli separated by a longer (3-day) interval. In the CA1 region of the hippocampus and in the lateral amygdala, neurons with this firing property link memories of events that occurred closely together in time. This is because the activated neurons remain highly excitable for a specific window of time after firing^{30,43}. The role of this neuronal population in itch and pain processing in the ACC, however, remains unclear. We were unable to manipulate these neurons in the present study because their inhibition caused other neurons with the second-highest level of excitability to be activated instead⁴⁴. Given the mutual inhibition of pain and itch, it is likely that these neurons are inhibitory interneurons that link pain and itch information. In the spinal cord, inhibitory neurons expressing the Olig-related transcription factor *Bhlhb5* act as gatekeepers that suppress the transmission of itch stimuli when they are activated by pain stimuli⁴⁵. The ACC also contains inhibitory interneurons that suppress pain, but it is unclear whether these interneurons are activated by itch information. Optogenetic activation of parvalbumin-positive inhibitory interneurons in the ACC reduced the hyperalgesia induced by complete Freund's adjuvant⁴⁶. In future studies, we hope to determine whether ACC neurons with excitability-based activation properties have a role in the mutual inhibition of pain and itch perception.

Our eGRASP data showing synaptic connections between ACC and MD neurons also suggest the intriguing possibility of crosstalk between pain and itch signals. Most neurons in the ACC and MD were modality-specific, with a very low proportion (<10%) of neurons activated by both pain and itch stimuli (Figs. 2, 3, Supplementary Fig. 9). It was interesting to find that the ACC neurons activated by itch stimulation received ~36% synaptic input from MD neurons activated by pain stimulation. The pain-specific neurons also showed a similar situation, with ~24% of their synaptic inputs coming from itch-specific MD neurons (Fig. 4). Under normal conditions, itch-specific MD presynaptic inputs are insufficient to functionally modulate pain-specific ACC neurons and pain-specific MD presynaptic inputs are insufficient to modulate itch-specific ACC neurons. It is plausible, however, that pathological states, such as chronic pain or itching, can induce circuit changes based on synaptic plasticity. Such circuit plasticity might explain the mechanism of allodynia or alloknesis.

In conclusion, we revealed that although pain and itch sensation are closely related, they are processed in the ACC by functionally distinct neuronal populations. The innate functionality of pain- or itch-specific ACC neurons is determined by their synaptic connections with presynaptic MD neurons. In addition, we identified a subset of ACC neurons activated by both stimuli, in a pattern likely based on excitability. It remains possible that both pain and itch sensation share certain common sub-circuits within the brain. In the future, we plan to further investigate the various circuits responsible for the higher-level functions of the ACC, including those specific for pain and itch detection, as well as the relationships between them.

Methods

Animals

Male C57BL/6NcrJlbg mice aged between 6 and 8 weeks were purchased from Orient Bio. Animals were housed in standard laboratory cages on a 12-hour light–dark cycle with access to food and water *ad libitum*. The mouse strains *Fos-tTA* (stock # 018306) and *tetO-H2BGFP* (stock # 005104) were purchased from The Jackson Laboratory and

used to generate double-transgenic TetTag mice⁴⁷. TetTag and Fos-tTA transgenic mice were fed a diet containing 0.04 g/kg doxycycline, except for during the Dox-withdrawal period. TRAP2 mice (stock # 030323) were used to label activated neurons⁴⁸. Ai14 reporter mice (stock # 007914) were used to visualize the regions of the thalamus pre-synaptic to the ACC in a cre-dependent manner⁴⁹. For TetTag mice, which are double transgenic and challenging to obtain, both male and female mice were used. To eliminate the potential influence of sex on experimental outcomes, males and females were evenly distributed across groups. In all other experiments, only male mice were utilized. All animal experiments were approved by the Institute of Laboratory Animal Resources of Seoul National University (SNU-I60919-2-2, SNU-150413-1).

Cannulation and drug infusion

Guide cannulas (24 gauge) were implanted bilaterally into the mouse anterior cingulate cortex (ACC; stereotaxic coordinates anteroposterior [AP] +0.7 mm, mediolateral [ML] ±0.3 mm, dorsoventral [DV] -1.7 mm) under ketamine/xylazine anesthesia. The mice were given at least 1 week to recover after cannula implantation. A 30-gauge injection cannula was inserted 0.2 mm lower than the guide cannula. For intra-ACC microinjection, 6-cyano-7-nitroquinoline-2,3-dione + tetrodotoxin (3 mM CNQX + 20 µM TTX in a total volume of 0.5 µl of saline) or vehicle (saline) was delivered bilaterally within 2 min using a pump. The cannula was kept in place for an additional 2 min after drug infusion. After the behavioral experiment completion, the mice were microinjected with ink and decapitated for confirmation of the injection sites.

Itch test

Pruritogens were always prepared fresh on the day of injection. Mice were briefly anesthetized with isoflurane and intradermally injected into the nape with histamine or chloroquine using a Hamilton syringe. Subsequently, the mice were transferred into a plexiglass chamber and their behavior was video-recorded from above for 30 min after awakening from anesthesia. An experimenter—blind to the experimental group of each mouse—manually counted the number of scratching bouts using the hind paws.

Pain test

Allogens were always prepared fresh on the day of injection. Mice were briefly anesthetized with isoflurane to facilitate the subcutaneous injection of formalin or capsaicin into the sole of the left hind paw using a Hamilton syringe. Care was taken to prevent any leakage of the injected solution. The mice were then transferred into an opaque plexiglass chamber with a transparent floor and their behavior was video-recorded from the bottom of the chamber for 1 h (formalin) or 15 min (capsaicin) after they awoke from anesthesia. Nociceptive responses, such as licking, flinching, and lifting of the injected paw, were manually measured by an experimenter blind to the experimental group of each mouse.

Virus production

We produced Adeno-Associated Viruses of serotype 2/1 (AAV2/1; a hybrid AAV particle with serotype 1 and 2 capsid features) using a procedure based on our earlier work³⁷. Specifically, AAV2/1 particles were generated from HEK293T cells that had been transfected with plasmids containing expression cassettes flanked by AAV2 ITR sequences, including p5E18, p5E18-RXCl, and pAd-DF6. The cells were cultured in 18 mL of Opti-MEM medium (GIBCO-BRL/Invitrogen, cat# 31985070) in 150-mm culture dishes. After three to four days, the culture medium was collected and centrifuged at 3000 rpm for 10 min. For purification, 1 mL of heparin-agarose suspension (Sigma, cat# H6508) was loaded into a poly prep chromatography column (Bio-Rad Laboratories, cat# 731-1550) and carefully applying the supernatant to

the column. The column was washed sequentially with 4 mL of buffer 4-150 (150 mM NaCl, 10 mM citrate buffer at pH 4) and 12 mL of buffer 4-400 (400 mM NaCl, 10 mM citrate buffer at pH 4). Virus particles were eluted with 4 mL of buffer 4-1200 (1.2 M NaCl, 10 mM citrate buffer at pH 4). The eluted solution was exchanged for PBS and concentrated using an Amicon Ultra-15 centrifugal filter unit (Millipore, cat# UFC910024). The viral titers were quantified through qRT-PCR. For AAV9, the viral vectors were produced and packaged by the IBS Virus Facility (https://centers.ibs.re.kr/html/virusfacility_en/). These vectors were prepared according to the facility's established protocols. AAV9 was used in Figs. 4 and 6 and their related experiments, and AAV2/1 was used in other experiments.

Experimental procedures with TetTag mice

The TetTag mice were habituated to handling for 8 days prior to their first injection. On the day before the last day of habituation, the mice were briefly anesthetized with isoflurane and their rostral backs were shaved with electric clippers. After the final day of habituation, the mice were provided standard food pellets without doxycycline for 4 days. On the day before their first injection, the mice were deprived of food to promote the intake of doxycycline-containing food the next day. One hour after histamine (20 µl, 40 mM in saline) injection as the first stimulus, mice received food pellets with a high dose of doxycycline (2 g/kg) to efficiently suppress any H2BGFP expression induced by nonspecific neuronal activity. On the next day, the mice instead received food pellets with a regular dose of doxycycline (0.04 g/kg). Histamine (20 µl, 40 mM in saline) or formalin (25 µl, 5% in saline) was injected as the second stimulus, either 6 h or 3 days after the first stimulus. The mice were then perfused for immunohistochemistry 90 min after the second injection.

Immunohistochemistry

Mice were anesthetized and transcardially perfused with phosphate-buffered saline (PBS, 0.01 M), followed by 4% paraformaldehyde (PFA) in PBS. The brains were collected, immersion-fixed in 4% PFA at 4 °C overnight, cryoprotected with 30% sucrose in PBS for 2 days at 4 °C, and embedded in an optimal cutting temperature (OCT) compound (Tissue-Tek, Sakura Finetek). Coronal sections (40 µm thick) were prepared using a cryostat, and every fourth section was collected in 50% glycerol in PBS. The sections were washed three times with PBS for 5 min each, incubated with a blocking solution (PBS containing 0.3% Triton X-100 [PBST] and 10% normal goat serum) for 30 min at room temperature. Subsequently, they were incubated with rabbit anti-c-Fos antibody (1:250, SantaCruz Biotechnology, Cat# sc-52) diluted in blocking solution for 2 days at 4 °C. The rat anti-c-Fos (1:500, Synaptic Systems, Cat# 226 017), rabbit anti-CaMKII (1:200, Abcam, Cat# ab52476), and guinea pig anti-GABA (1:200, EMD Millipore, Cat# MAB360) antibodies were used for double immunostaining. The sections were washed four times with PBS containing 0.3% Triton X-100 (PBST) for 10 min each, incubated with fluorophore-conjugated secondary antibodies (1:500) diluted in the blocking solution for 2 h at room temperature, followed by four additional washes with PBST for 10 min each. The sections were then incubated with 4',6-diamidino-2-phenylindole (DAPI, 0.2 µg/mL, Invitrogen) in PBS for 10 min at room temperature, transferred onto glass slides, and mounted with VECTASHIELD (Vector Laboratories). Imaging of the sections were conducted with an LSM700 (Carl Zeiss) confocal microscope or a fluorescence microscope, and the resulting images were analyzed with IMARIS or ImageJ software.

For the analysis of the TetTag mice, the proportion of neurons expected to show double labeling based on chance alone was calculated as previously described according to the following equation: Chance level = ((number of H2BGFP+ neurons) / (number of DAPI+ neurons)) × ((number of Fos+ neurons) / (number of DAPI+ neurons))⁵⁰.

Heatmap generation and visualization for fos immunohistochemistry

Microscopic images were acquired systematically by identifying the center of gravity for each fos (+) cell and representing them as pivotal data points. The precise alignment of these data points was achieved through geometric transformations, encompassing rotation, isotropic scaling, translation, and linear scaling. These transformations were benchmarked against the boundary data points obtained from the ACC region across distinct mouse specimens and their affiliated subsets. The alignment process involved two main phases. First, a rotational adjustment and isotropic scaling were carried out. This was done using a set of vertical reference vectors that were taken from specific pairs of boundary data points. This step ensured that the image was rotated and scaled correctly. After this, the dataset was scaled in width to match a pre-established average width, making sure there was consistency throughout the data. Once the scaling was done, modifications were made to the x and y coordinates. This made sure the data were placed right at the center of the designated matrix. After alignment, the 2D coordinates representing the ACC fos (+) cells were transmuted into a binary image format. These binary images from the dataset were integrated by summing individual layers and subsequently averaging them, yielding a comprehensive composite image. A Gaussian filter was then applied to enhance the clarity and presentation of the composite. Further refinement and resolution optimization was achieved by interpolating the smoothed data. For visualization, a heatmap was created using the jet colormap with the color intensity gradient set between the 0 and 0.025 thresholds. Post interpolation, this specific intensity range was employed, serving as an all-encompassing absolute scale for the presented data.

Integrated microendoscope imaging

For in vivo 1-photon calcium imaging, we made use of integrated microendoscopes, called miniscopes. The miniscope V3 was used for these experiments. A CMOS imaging sensor (Aptina, MT9V032) was printed on a CMOS imaging sensor PCB (available at https://github.com/daharoni/Miniscope_CMOS_Imaging_Sensor_PCB) and soldered to a coaxial cable (RG-174/U(50Ω)). A Luxeon SMD blue LED (P/N LXML-PB01-0030) soldered to an excitation LED PCB was integrated into the main body of the microscope with the CMOS imaging sensor PCB. As optic tools, a 5 mm Dia. x 12.5 mm FL, MgF2 Coated, Achromatic Doublet Lens (Edmund Optics, 49-923), an excitation filter (Chroma, ET470/40×), an emission filter (Chroma, ET525/50 m), and a dichroic mirror (Chroma, T495lpxr) were also integrated into the main body of the miniscope. A 3.0-mm diameter N-BK7 half-ball lens (Edmund Optics, 47-269) was attached with optical adhesive (Edmund Optics, 55-084) and cured with UV light. The integrated miniscope was linked to a commutator (PANLINK, PSR-C6) to prevent the coiling of its cable.

Stereotaxic surgeries for calcium imaging

For virus injections, mice were anesthetized by intraperitoneal injection of ketamine/xylazine solution and placed in a stereotaxic apparatus (Stoelting Co.). AAV2/1-EFlα-GCaMP6f was injected into the right ACC (AP 0.7 mm, ML 0.25 mm, DV 1.9 mm) using a 33-gauge needle with a Hamilton syringe. After a 2-min rest during which the injection needle's tip was placed 0.1 mm below the target location, the tip was returned to the target location to inject 0.5 μl of virus with a 0.125 μl/min flow rate. The needle was then removed slowly 7 min after the injection. One week after AAV injection, a 2.0-mm diameter GRIN lens (Go!Foton, CLHS200GFT027) was implanted over the ACC. The mice were anesthetized by intraperitoneal injection of ketamine/xylazine and then positioned in a stereotaxic apparatus. The craniotomy for the GRIN lens was 2.0–2.1 mm in diameter to leave a minimal gap between the GRIN lens and the skull. A cylindrical column of neocortex was aspirated with a blunt 27-gauge needle using

saline until the plane of the subfornical artery was located. After bleeding stopped, the blood clot was gently removed and the GRIN lens was implanted (DV 1.7 mm) into the hole. Screws were then added to the skull for anchoring. The GRIN lens and its screws were fixed with Loctite and dental cement. After curing, a biocompatible Silastic elastomer (Kwik-Sil, World Precision Instruments, Berlin Germany) was added around the GRIN lens to protect it from scratches. Three weeks after the GRIN lens was implanted, the mice were anesthetized again by intraperitoneal injection of ketamine/xylazine and then positioned in a stereotaxic apparatus for baseplating surgery. A baseplate attached to a miniscope was placed on the GRIN lens and fixed with dental cement at the angle with the best GCaMP6f signal. The GRIN lens was then covered by a cap with screws on the baseplate until the day of calcium imaging.

Behavioral experiment procedures with miniscopes

After the mice finished all the stereotaxic surgeries, including baseplating, they were monitored for 1 week. The mice were caged individually. All training and testing were conducted during the light cycle. The mice were habituated to the coaxial cable and miniscope for 5 days without isoflurane anesthesia. Each habituation step lasted 10 min with 30-min rest sessions. Only one miniscope was used per mouse. For the first two days, habituation was hands-only. Then, for the next two days, the mice underwent miniscope attachment habituation, in which the miniscopes were attached to baseplates on their heads with screws and the mice were delivered to a new cage where they could move about freely for 30 sec. Then, the miniscopes were detached and the mice were delivered back to the cage where they could move freely for another 30 sec. This procedure was performed repeatedly for 10 min. On the last day of habituation, after the miniscopes were attached with isoflurane anesthesia and after a 30-min rest, the mice were delivered from a new cage to an anesthesia box for 30 sec.

Calcium imaging of freely moving mice

On the day of calcium imaging, the mice were habituated in a rack for 30 min with their miniscopes and commutators attached. Calcium imaging was performed during the light cycle, and calcium events were captured with DAQ software (available at https://github.com/daharoni/Miniscope_DAQ_Software) at 15 frames/s with the CMOS sensor set at maximum gain. To prevent photobleaching, the LED power was set to between 3–10% and each mouse received the same LED power during all three calcium imaging sessions (at 0 h, 72 h, and 78 h). The commutators were connected to the DAQ board so the signal from the CMOS could be sent to the software on a computer. After 5 min of baseline imaging, the mice were anesthetized with isoflurane and injected with histamine into the subcutaneous tissues of the nape of the neck or with formalin into the subcutaneous tissues of the left hind foot. After 5 min of recovery from the isoflurane, the calcium responses to itch or pain were imaged for 10 min. After calcium imaging, the mice were detached from their miniscopes and returned to their home racks. These calcium imaging sessions were repeated three times per mouse. The LED was off except during the imaging steps.

Calcium imaging data acquisition, processing, and cell sorting

Calcium transients captured using DAQ software and hardware (Labmaker or Sierra Circuits, v3.2) and saved in the .avi video format. Those videos were processed by MINIPipe⁵¹ and the individual session videos were combined. This combined video was subjected to several analyses, pre-processing, and neural activity identification. CellReg was used to track detected neural populations across multiple time points⁵². Neural population classification and signal processing was performed using custom MATLAB code. Machine learning classifications of the neural signals were performed using WEKA⁵³.

Registration of the calcium imaging movies

Preprocessing. The primary objective of preprocessing was to eliminate noise to enhance the signal-to-noise ratio (SNR). An anisotropic diffusion denoising operation was performed on the raw image frames to remove the grainy noise inherent in the single-photon system while preserving the boundary between the foreground and background⁵⁴. Additionally, a morphological opening operation was conducted using the background estimator to remove structures smaller than the desired structural element⁵⁵. For motion artifact and distortion removal, the image video was decomposed into stable and unstable sections. The Kanade–Lucas–Tomasi (KLT) tracker was used to estimate the displacement of potential corner-like features between two adjacent frames⁵⁶. In stable sections, motion was approximated using small translational displacements, while unstable sections contained large general deformations. The fast Lucas-Kanade tracker was used, which could be efficiently run in parallel on multiple sections to correct for small translational displacements within each stable section⁵⁷. The diffeomorphic log-demon image registration method was performed for handling large deformations while preserving local geometric properties⁵⁸. To align all the stable sections, KLT and LogDemons were applied to the sectional images in a pairwise manner. The pairwise similarity of the sectional images was computed, generating a directed graph between all the sectional images. Similar sectional images that formed a cluster in the graph were combined, while this iteration was repeated until all sectional images were combined. Subsequently, the estimated displacement field was applied to each frame within the same stable section. To register the individual frames within each unstable section, the extraction of the sectional images and their registration were performed similarly to the stable section.

Neural Signal Extraction. During the seed cleaning process, an over-complete set of seeds containing all potential centers of real regions of interest (ROIs) was generated, including false positives. To clean this set more effectively, a two-component Gaussian mixture model (GMM) was utilized. It was applied to the peak-valley differences in the corresponding traces of the seeds. Typically, the traces of real neurons exhibit larger fluctuations than those of false-positive seeds of non-neurons. The GMM effectively removed most background false positives while retaining real neurons. To further eliminate the remaining false positives, such as those exhibiting abnormal background fluctuations or hemodynamics, trained recurrent neural networks (RNNs) with long-short term memory (LSTM) modules were used as classifiers for calcium spike^{59,60}. In cases where multiple seeds were found within a single ROI, potentially redundant seeds were merged by computing the temporal similarity of seeds within their neighborhoods and preserving those with the highest intensity. A simplified spatiotemporal CNMF was used to separate regions of interest (ROIs) and corresponding calcium traces⁶¹. To update the spatial footprints of individual ROIs and temporal traces with deconvolved spike trains, iterative spatial and temporal optimizations were performed. Unlike previous CNMF or CNMF-E methods, where the spatial footprints were sequentially updated and subtracted from the previous residuals, the spatial footprints in this approach were extracted from the original data and remained independent of previous iterations.

Validation of accuracy of cell registration. Several techniques were employed to validate cell registration across multiple sessions at the cell pair and cell register levels. First, exclusivity and transitivity were checked to ensure the consistency of the model with the data. Exclusivity indicated that once a cell from session 1 was paired with a cell from session 2, no other cell from session 2 could be paired with it. Transitivity indicated that once a cell from session 1 is paired with a cell from session 2, and the cell from session 2 is paired with a cell from session 3, then cells from sessions 1 and 3 must also be paired. To measure exclusivity, the focus was on cells whose pairing candidates

had a P_{same} value > 0.5 in another session. The distribution of P_{same} was calculated across all additional pairing candidates for these cells. To measure transitivity, P_{same} distributions were calculated for cell pairs from two different sessions, each having a P_{same} value > 0.5 with the same candidate from a third session. No differences in transitivity were observed among the three different models. CellReg also provided various validation metrics. The cell-to-index map displayed the mapping of each registered cell to the indices in each registered session. Cell scores indicated registration quality metrics for all registered cells, including true positive, true negative, and exclusivity scores. A logical vector indicated whether a cell was within the imaged field of view in all sessions. Centroids of registered cells represented average centroid locations across all registered cells. Corrected centroid locations represented transformed centroid locations of all registered cells in each session. Corrected spatial footprints depicted aligned spatial footprints of all registered cells in each session. While all these parameters were considered, only two criteria were primarily used: p_{matching} and cell score. These criteria demonstrated the overall distribution of the analysis output rather than specific values such as averages or variances. In an imaging environment using mini-endoscopes, a certain upper limit of variance was considered more likely to occur within the image set rather than isolated outliers in the overall matching. This was because significant distortion was unlikely, considering factors such as neodymium magnets. Based on this assessment, selections were made based on p_{matching} alone when the cell score was adequately secured. However, for datasets with low cell scores due to imaging and surgical conditions, stability in criteria was preferred.

Machine learning classification

Machine learning classification of neural signals was processed on Weka (Eibe Frank et al., 2016). Stochastic Gradient Descent (SGD) was employed as the optimization algorithm for training the model, leveraging Weka's built-in implementation. The SGD algorithm was utilized to optimize model parameters. SGD minimizes the loss function by iteratively updating the parameters. Statistical evaluations of more machine learning classifiers are in Supplementary Table 1. To validate the model's robustness, a 10-fold cross-validation was applied during training. This ensures that the model's performance is not overly dependent on a specific data split.

Stereotaxic surgery for GRASP experiments

Mice were anesthetized with a ketamine/xylazine solution and positioned on a stereotaxic apparatus (Stoelting Co.). The virus mixture was injected into target regions through a 32-gauge needle with a Hamilton syringe at a rate of 0.1 $\mu\text{l}/\text{min}$ up to a total injection volume per site of 0.3 μl . The needle tip was positioned 0.1 mm below the target coordinates for 2 min right before the injection. After the injection was completed, the needle remained in place for an additional 7 min and then it was slowly withdrawn. The stereotaxic coordinates for each target site were as follows: anterior cingulate cortex (AP: +0.8/ ML: ± 0.3 / DV: -1.8) and mediodorsal thalamic nucleus (AP: -0.9/ ML: ± 0.45 / DV: -3.25).

IEG-based double tagging system

Two different activity-dependent tagging systems were used to label neurons activated by both itch stimuli and pain stimuli. In the TRAP2 (FoscreERT2) system, viral constructs were induced in a Cre recombinase-dependent manner. 4-OHT was delivered by intraperitoneal injection 30 min before itch stimulation to flip the double-floxed inverted gene. After inversion, the viral constructs were constitutively expressed from the EF1 α promoter. In the TetTag system, Fos-rtTA was combined with a tetracycline-responsive element 3rd generation (TRE3G) promoter-based Tet-On labeling strategy. In this system, when rtTA proteins are expressed in fos-expressing neurons,

the rtTA binds to the TRE3G promoter in the presence of doxycycline. Doxycycline was delivered by intraperitoneal injection 2 hours before pain stimulation. This induced expression of the viral constructs from the TRE3G promoter.

Dual-eGRASP sample preparation and confocal imaging

All viruses used for dual-eGRASP were confirmed in prior reports^{37,38}. Perfused brains were fixed with 4% paraformaldehyde in PBS overnight at 4 °C and dehydrated in 30% sucrose in PBS for 2 days at 4 °C. Brains were sliced into 50 µm sections for dual-eGRASP analysis. Sections were mounted in Vectashield mounting medium (H-1000; Vector Laboratories). For dual-eGRASP analysis, the ACC dendrites were imaged in Z-stacks using a Leica SP8 confocal microscope with a 63x objective and distilled water immersion.

Dual-eGRASP image analysis

IMARIS software (Bitplane, Zurich, Switzerland) was used to process confocal images and perform 3D dendritic reconstructions. Before the analysis, experimenters were blind to all image samples to avoid bias. Cyan or yellow eGRASP signals were marked as spheres in IMARIS while hiding the iRFP670 and mScarlet-1 fluorescent signals. Cyan and yellow eGRASP puncta that appeared on dendrites were manually counted⁶².

Behavioral experimental procedures using the Tet-Off system in Fos-tTA mice

For activity-dependent expression of hM4Di, which is an inhibitory designer receptor exclusively activated by a designer drug (DREADD), we used an AAV (serotype 1/2) capable of expressing both hM4Di and emerald GFP (hM4Di-P2A-emGFP) under the tetO promoter. To confirm that the AAV expressing the inhibitory DREADD was injected properly, we co-injected an AAV (serotype 1) expressing nuclear-localized mCherry (n-mCherry) under the control of the CaMKII promoter. The mixture of these two AAVs [2:8 v/v = AAV expressing n-mCherry (3.0×10^{11} gc/ml): AAV expressing inhibitory DREADD (2.1×10^{12} gc/ml)] was injected bilaterally into the ACC of Fos-tTA mice (AP + 0.7 mm, ML ± 0.3 mm, DV - 1.7 mm, 0.5 µl/side) during stereotaxic surgery (Stoelting Co.). One week after the stereotaxic surgery, the mice were habituated to handling for 5 days. On the day before the final habituation session, the mice were briefly anesthetized with isoflurane and the rostral part of the back was shaved with electric clippers. After the final habituation session, the mice were provided standard food pellets without doxycycline for 4 days. Then, the day before stimulus injection, the mice were deprived of food to promote intake of doxycycline-containing food the next day. One hour after histamine (20 µl, 40 mM in saline) or formalin (10 µl, 1% in saline) injection, the mice were given food pellets containing high-dose doxycycline (2 g/kg) to efficiently suppress the hM4Di expression induced by nonspecific neuronal activity. The next day, the food pellets were changed to regular-dose doxycycline (0.04 g/kg). Three days after stimulus injection, the mice were given intraperitoneal injections of clozapine-N-oxide (CNO, 0.1 mg/kg) or saline vehicle 30 min before subjecting them to itch or pain tests. After the behavioral experiments, the mice were decapitated to confirm the expression of the inhibitory DREADD. Their brains were collected and processed in the same manner as for immunohistochemistry, with the omission of the blocking and antibody steps.

Behavioral experimental procedures using the Tet-On system in WT mice

For activity-dependent expression of hM4Di and hM3Dq, a combination of two AAVs (serotype 9), fos::rtTA with TRE3G::hM4Di-mCherry, or fos::rtTA with TRE3G::hM3Dq-mCherry, was used in WT mice. The AAV mixture [1:1 v/v = fos::rtTA (4.0×10^{11} gc/ml): TRE3G::hM4Di-

mCherry (2.1×10^{12} gc/ml), 1:1 v/v = fos::rtTA (4.0×10^{11} gc/ml): TRE3G::hM3Dq-mCherry (5.6×10^{12} gc/ml)] was injected bilaterally into the ACC of WT mice (AP + 0.7 mm, ML ± 0.3 mm, DV - 1.7 mm, 0.5 µl/side) during stereotaxic surgery (Stoelting Co.). After three weeks post-stereotaxic surgery, the mice were briefly anesthetized with isoflurane, and their nape shaved using electric clippers. The next day, 2 h after intraperitoneal Dox (50 mg/kg in saline) injection, histamine (20 µl, 40 mM in saline) or formalin (10 µl, 5% in saline) was injected into the left side of the nape or left hind paw, respectively. After 2 d of stimulus injection, the mice were injected intraperitoneally with CNO (10 mg/kg) or saline 30 min before itching or pain tests. For the inhibitory hM4Di experiments, chloroquine (20 µl, 100 µg in saline) and capsaicin [10 µl, 1.5 µg in the vehicle (10% EtOH + 10% DMSO + 80% saline)] were used for the itch and pain tests, respectively. In the activating hM3Dq experiments, itch and pain tests were first conducted without any stimulus. However, 2 days later, intraperitoneal injections of CNO (10 mg/kg) or saline were administered again. Weak histamine (20 µl, 8 mM in saline) and weak formalin (10 µl, 0.5% in saline) were injected for the itch and pain tests, respectively, 30 min after the CNO injection. After the behavioral experiments, the mice were decapitated to confirm the expression of hM4Di-mCherry and hM3Dq-mCherry. Their brains were collected and processed similarly to immunohistochemistry, excluding the blocking and antibody steps.

Freezing-like behavior analysis

To measure freezing level without or with injecting algogenic substances or pruritogens, the differences between frames in recorded video files were compared. As mice adapt to the chamber, their movements slow down. To avoid considering this adaptation as freezing, only behavioral recordings of 5 min immediately after they entered the chamber were used for analysis of the freezing level. First, the mean squared error (MSE) algorithm was used to score the differences between adjacent frames. If the MSE value between two adjacent frames fell below a certain threshold, the mice were considered frozen at the moment. The accuracy of this threshold in detecting freezing behavior was confirmed through visual inspection of sample videos. Finally, the percentage of time spent freezing was calculated using the timestamp data acquired simultaneously with the video frames.

Electrophysiology

Mice were deeply anesthetized by intraperitoneal injection of ketamine. Transcardial perfusion was the performed using an ice-chilled sucrose solution containing (in mM): 210 sucrose, 3 KCl, 26 NaHCO₃, 1.25 NaH₂PO₄, 5 MgSO₄, 10 D-glucose, 3 sodium ascorbate, and 0.5 CaCl₂, saturated with 95% O₂ and 5% CO₂. Following this, the brain was isolated and immediately placed in the ice-chilled sucrose solution for approximately 30 s. Two to three coronal slices, 350 µm thick, containing the ACC were prepared employing a vibratome (Leica, VT1200S). The slices were transferred to the recovery chamber filled with artificial cerebrospinal fluid (ACSF) containing (in mM): 124 NaCl, 3 KCl, 26 NaHCO₃, 1.25 NaH₂PO₄, 2 MgSO₄, 10 D-glucose, and 2 CaCl₂ (carbonated with 95% O₂ and 5% CO₂) for 30 min at 32-34 °C. The recovery chamber temperature was adjusted to 28-30 °C and maintained until the recording was completed.

Whole-cell recordings were performed in a recording chamber constantly perfused with ACSF at 3-4 ml/min at 32 °C. Borosilicate glass pipettes with a resistance of 3-7 MΩ were used and filled with K-gluconate internal solution consisting of (in mM): 8 NaCl, 130 K-gluconate, 10 HEPES, 0.5 EGTA, 4 Mg-ATP, 0.3 Na₃-GTP, 5 KCl, and 0.1 spermine. The pH was adjusted to 7.2-7.3 with KOH, and the osmolarity was set to 285-290 mOsm/l. Signals were obtained using a Multiclamp 700B amplifier (Molecular Devices, US) and digitized utilizing Digidata 1550 (Molecular Devices, US) at a sampling rate of 20 kHz (filtered at 2 kHz).

mCherry (+) neurons in the ACC were visualized using an Axio Examiner D1 microscope (40x, ZEISS, US). Excitation light was provided by a CoolLED pE340 fura (CoolLED, UK), and real-time images were captured with a sCMOS digital camera and sent to the computer. Neurons were voltage-clamped at -70 mV, and spontaneous responses were monitored for at least 5 min after establishing the whole-cell configuration to allow for stabilization owing to internal solution influx. After stabilization, the baseline resting membrane potential (mV) was measured at $I = 0$. Depolarizing currents of 500 ms were applied to the neuron with an inter-trial interval of 6 s. The current intensity was increased by 20 pA, ranging from 0–300 pA. Subsequently, neurons were voltage-clamped at -70 mV while the recording chamber was perfused with ACSF containing CNO (5–10 μ M, Sigma-Aldrich, C0832) for 10 min. Following this, the resting membrane potential and neuronal firing in response to the current injection were measured again as described above. To examine CNO effect, the number of action potentials (APs) evoked by the same current intensity was compared before and after the CNO application. The minimum current that elicited at least 6 APs during the baseline period was selected for comparison. Neurons that depolarized above -50 mV were excluded from the analysis.

Data analysis

Statistical comparisons were made using unpaired t-tests, paired t-tests, repeated-measures two-way ANOVAs (with Bonferroni tests for post-hoc comparisons), and Mann–Whitney U tests. All data are presented as means \pm standard error of the mean (SEM) or as box-and-whiskers plots (5–95% percentile). In all cases, $p < 0.05$ was considered statistically significant.

Reporting summary

Further information on research design is available in the Nature Portfolio Reporting Summary linked to this article.

Data availability

All the other data are available within the article and its Supplementary Information. Source data are provided with this paper.

Code availability

Analysis code is available at this GitHub or other repository: Miniscope DAQ software (https://github.com/daharoni/Miniscope_DAQ_Software). MINIPIPE v2-alpha (<https://github.com/JinghaoLu/MINIPIPE>). CellReg ver 1.4.9 (<https://github.com/zivlab/CellReg>). Customized MATLAB code (https://github.com/yoplaitlid/pain_itch); (<https://doi.org/10.5281/zenodo.14408248>) Weka 3.8.4 (<https://sourceforge.net/projects/weka/files/weka-3-8/3.8.4/>) Customized python code (https://github.com/chuljkwak/pain_itch_freezing); (<https://doi.org/10.5281/zenodo.14435325>).

References

- Xiu, J. et al. Visualizing an emotional valence map in the limbic forebrain by TAI-FISH. *Nat. Neurosci.* **17**, 1552–1559 (2014).
- Han, C. J. et al. Trace but not delay fear conditioning requires attention and the anterior cingulate cortex. *PNAS* **100**, 13087–13092 (2003).
- Jeon, D. et al. Observational fear learning involves affective pain system and Ca v 1.2 Ca 2+ channels in ACC. *Nat. Neurosci.* **13**, 482–488 (2010).
- Valentini, E. The role of anterior insula and anterior cingulate in empathy for pain. *J. Neurophysiol.* **104**, 584–586 (2010).
- Mochizuki, H. et al. Time course of activity in itch-related brain regions: a combined MEG-fMRI study. *J. Neurophysiol.* **102**, 2657–2666 (2009).
- Frankland, P. W., Bontempi, B., Talton, L. E., Kaczmarek, L. & Silva, A. J. The involvement of the anterior cingulate cortex in remote contextual fear memory. *Science* **304**, 881–883 (2004).
- Frankland, P. W. & Bontempi, B. The organization of recent and remote memories. *Nat. Rev. Neurosci.* **6**, 119–130 (2005).
- Bush, G., Luu, P. & Posner, M. I. Cognitive and emotional influences in anterior cingulate cortex. *Trends Cogn. Sci.* **4**, 215–222 (2000).
- Bliss, T. V. P., Collingridge, G. L., Kaang, B.-K. & Zhuo, M. Synaptic plasticity in the anterior cingulate cortex in acute and chronic pain. *Nat. Rev. Neurosci.* **17**, 485–496 (2016).
- Vogt, B. A. Pain and emotion interactions in subregions of the cingulate gyrus. *Nat. Rev. Neurosci.* **6**, 533–544 (2005).
- Berridge, K. C. Affective valence in the brain: modules or modes? *Nat. Rev. Neurosci.* **20**, 225–234 (2019).
- Lu, J.-S., Chen, Q.-Y., Zhou, S., Inokuchi, K. & Zhuo, M. Dual roles of anterior cingulate cortex neurons in pain and pleasure in adult mice. *Mol. Brain* **11**, 72 (2018).
- Shackman, A. J. et al. The integration of negative affect, pain, and cognitive control in the cingulate cortex. *Nat. Rev. Neurosci.* **12**, 154–167 (2011).
- Wu, L.-J., Kim, S. S., Li, X., Zhang, F. & Zhuo, M. Sexual attraction enhances glutamate transmission in mammalian anterior cingulate cortex. *Mol. Brain* **2**, 9 (2009).
- Braz, J., Solorzano, C., Wang, X. & Basbaum, A. I. Transmitting pain and itch messages: a contemporary view of the spinal cord circuits that generate gate control. *Neuron* **82**, 522–536 (2014).
- Barry, D. M. et al. Exploration of sensory and spinal neurons expressing gastrin-releasing peptide in itch and pain related behaviors. *Nat. Commun.* **11**, 1397 (2020).
- Koga, K. et al. Glutamate acts as a neurotransmitter for gastrin releasing peptide-sensitive and insensitive itch-related synaptic transmission in mammalian spinal cord. *Mol. Pain.* **7**, 47 (2011).
- Liu, T. & Ji, R.-R. New insights into the mechanisms of itch: are pain and itch controlled by distinct mechanisms? *Pflug. Arch.* **465**, 1671–1685 (2013).
- Han, L. et al. A subpopulation of nociceptors specifically linked to itch. *Nat. Neurosci.* **16**, 174–182 (2013).
- Akiyama, T. & Carstens, E. Spinal Coding of Itch and Pain. in *Itch: Mechanisms and Treatment* (eds. Carstens, E. & Akiyama, T.) (CRC Press/Taylor & Francis, Boca Raton (FL), 2014).
- Davidson, S. & Giesler, G. J. The multiple pathways for itch and their interactions with pain. *Trends Neurosci.* **33**, 550–558 (2010).
- Deng, J. et al. The parabrachial nucleus directly channels spinal nociceptive signals to the intralaminar thalamic nuclei, but not the amygdala. *Neuron* **107**, 909–923.e6 (2020).
- Descalzi, G. et al. Cortical GluK1 kainate receptors modulate scratching in adult mice. *J. Neurochem.* **126**, 636–650 (2013).
- Devinsky, O., Morrell, M. J. & Vogt, B. A. Contributions of anterior cingulate cortex to behaviour. *Brain* **118**, 279–306 (1995).
- Chen, T. et al. Postsynaptic potentiation of corticospinal projecting neurons in the anterior cingulate cortex after nerve injury. *Mol. Pain.* **10**, 33 (2014).
- Ko, H.-G. et al. Rapid turnover of cortical NCAM1 regulates synaptic reorganization after peripheral nerve injury. *Cell Rep.* **22**, 748–759 (2018).
- Josselyn, S. A. & Frankland, P. W. Memory allocation: mechanisms and function. *Annu. Rev. Neurosci.* **41**, 389–413 (2018).
- Zhou, Y. et al. CREB regulates excitability and the allocation of memory to subsets of neurons in the amygdala. *Nat. Neurosci.* **12**, 1438–1443 (2009).
- Han, J.-H. et al. Neuronal competition and selection during memory formation. *Science* **316**, 457–460 (2007).
- Cai, D. J. et al. A shared neural ensemble links distinct contextual memories encoded close in time. *Nature* **534**, 115–118 (2016).

31. Commerford, S. L., Carsten, A. L. & Cronkite, E. P. Histone turnover within nonproliferating cells. *PNAS* **79**, 1163–1165 (1982).
32. Barros, V. N. et al. The pattern of c-Fos expression and its refractory period in the brain of rats and monkeys. *Front. Cell. Neurosci.* **9**, 72 (2015).
33. Zhang, T.-T. et al. Potentiation of synaptic transmission in Rat anterior cingulate cortex by chronic itch. *Mol. Brain* **9**, 73 (2016).
34. Oh, J., Lee, C. & Kaang, B.-K. Imaging and analysis of genetically encoded calcium indicators linking neural circuits and behaviors. *Korean J. Physiol. Pharm.* **23**, 237 (2019).
35. Xue, M. et al. Mapping thalamic-anterior cingulate monosynaptic inputs in adult mice. *Mol. Pain* **18**, 17448069221087034 (2022).
36. Kuramoto, E. et al. Individual mediadorsal thalamic neurons project to multiple areas of the rat prefrontal cortex: A single neuron-tracing study using virus vectors. *J. Comp. Neurol.* **525**, 166–185 (2017).
37. Choi, J.-H. et al. Interregional synaptic maps among engram cells underlie memory formation. *Science* **360**, 430–435 (2018).
38. Choi, D. I. et al. Synaptic correlates of associative fear memory in the lateral amygdala. *Neuron* **109**, 2717–2726.e3 (2021).
39. Koga, K. et al. Coexistence of two forms of LTP in ACC provides a synaptic mechanism for the interactions between anxiety and chronic pain. *Neuron* **85**, 377–389 (2015).
40. Acuña, M. A., Kasanetz, F., De Luna, P., Falkowska, M. & Nevian, T. Principles of nociceptive coding in the anterior cingulate cortex. *Proc. Natl Acad. Sci. USA* **120**, e2212394120 (2023).
41. Liu, Y. et al. Oxytocin promotes prefrontal population activity via the PVN-PFC pathway to regulate pain. *Neuron* **111**, 1795–1811.e7 (2023).
42. Li, A. et al. Disrupted population coding in the prefrontal cortex underlies pain aversion. *Cell Rep.* **37**, 109978 (2021).
43. Rashid, A. J. et al. Competition between engrams influences fear memory formation and recall. *Science* **353**, 383–387 (2016).
44. Han, J.-H. et al. Selective erasure of a fear memory. *Science* **323**, 1492–1496 (2009).
45. Kardon, A. P. et al. Dynorphin acts as a neuromodulator to inhibit itch in the dorsal horn of the spinal cord. *Neuron* **82**, 573–586 (2014).
46. Kang, S. J. et al. Bidirectional modulation of hyperalgesia via the specific control of excitatory and inhibitory neuronal activity in the ACC. *Mol. Brain* **8**, 81 (2015).
47. Tanaka, K. Z. et al. Cortical representations are reinstated by the hippocampus during memory retrieval. *Neuron* **84**, 347–354 (2014).
48. DeNardo, L. A. et al. Temporal evolution of cortical ensembles promoting remote memory retrieval. *Nat. Neurosci.* **22**, 460–469 (2019).
49. Madisen, L. et al. A robust and high-throughput Cre reporting and characterization system for the whole mouse brain. *Nat. Neurosci.* **13**, 133–140 (2010).
50. Reijmers, L. G., Perkins, B. L., Matsuo, N. & Mayford, M. Localization of a Stable Neural Correlate of Associative Memory. *Science* **317**, 1230–1233 (2007).
51. Lu, J. et al. MINIPipe: a miniscope 1-photon-based calcium imaging signal extraction pipeline. *Cell Rep.* **23**, 3673–3684 (2018).
52. Sheintuch, L. et al. Tracking the same neurons across multiple days in ca2+ imaging data. *Cell Rep.* **21**, 1102–1115 (2017).
53. Appendix B - The WEKA workbench. in *Data Mining (Fourth Edition)* (eds. Witten, I. H., Frank, E., Hall, M. A. & Pal, C. J.) 553–571 (Morgan Kaufmann, 2017). <https://doi.org/10.1016/B978-0-12-804291-5.00024-6>.
54. Perona, P. & Malik, J. Scale-space and edge detection using anisotropic diffusion. *IEEE Trans. Pattern Anal. Mach. Intell.* **12**, 629–639 (1990).
55. Serra, J. & Vincent, L. An overview of morphological filtering. *Circuits Syst. Signal Process* **11**, 47–108 (1992).
56. Shi, J. & Tomasi. Good features to track. in 1994 Proceedings of IEEE Conference on Computer Vision and Pattern Recognition 593–600 <https://doi.org/10.1109/CVPR.1994.323794> (1994).
57. Lucas, B. D. & Kanade, T. An iterative image registration technique with an application to stereo vision. *Proc. 7th Int. Jt. Conf. Artif. Intell.* **2**, 674–679 (1981).
58. Vercauteren, T., Pennec, X., Perchant, A. & Ayache, N. Diffeomorphic demons: efficient non-parametric image registration. *Neuroimage* **45**, S61–S72 (2009).
59. Hochreiter, S. & Schmidhuber, J. Long short-term memory. *Neural Comput.* **9**, 1735–1780 (1997).
60. LeCun, Y., Bengio, Y. & Hinton, G. Deep learning. *Nature* **521**, 436–444 (2015).
61. Pnevmatikakis, E. A. et al. Simultaneous denoising, deconvolution, and demixing of calcium imaging data. *Neuron* **89**, 285–299 (2016).
62. Choi, D. I. & Kaang, B.-K. Interrogating structural plasticity among synaptic engrams. *Curr. Opin. Neurobiol.* **75**, 102552 (2022).

Acknowledgements

We thank Dr. Jin-Hee Han for the critical discussion and Dr. Jooyoung Kim for the technical assistant. This study was funded by the NRF (2018R1C1B6008530 and 2021R1A2C1013092 to H-GK, 2022R1F1A1071248 to J-HL, and NRF-2012R1A3A1050385 to B-KK), Canadian Institute for Health Research (CIHR) (PJT-148748 and PJT-419286 to MZ), and Institute for Basic Science (IBS-R001-D3 to B-KK).

Author contributions

H-G.K. designed the studies, carried out the molecular and behavioral experiments, and outlined and wrote the manuscript. D.I.C. and J.E.C. performed the GRASP experiments. S.H. conducted behavioral and immunohistological experiments. H.J. prepared and injected the AAVs. C.K. participated in behavioral experiments and data analysis. D.H.H. conducted electrophysiological experiments and participated in AAV injection. J-N.K. analyzed immunostained images and behavioral experiment data. C.L., J.O., Jiah L., and H.J. performed the in vivo miniscope imaging experiments. S.Y. participated in behavioral experiments. Jaehyun L. made the AAVs. K.L., J-H.L., M.Z., and B-K.K. participated in the interpretation of the data and wrote the manuscript. B-K.K. supervised the experiments.

Competing interests

The authors declare no competing interests.

Additional information

Supplementary information The online version contains supplementary material available at <https://doi.org/10.1038/s41467-025-57041-z>.

Correspondence and requests for materials should be addressed to Hyoung-Gon Ko or Bong-Kiun Kaang.

Peer review information *Nature Communications* thanks the anonymous reviewers for their contribution to the peer review of this work. A peer review file is available.

Reprints and permissions information is available at <http://www.nature.com/reprints>

Publisher's note Springer Nature remains neutral with regard to jurisdictional claims in published maps and institutional affiliations.

Open Access This article is licensed under a Creative Commons Attribution-NonCommercial-NoDerivatives 4.0 International License, which permits any non-commercial use, sharing, distribution and reproduction in any medium or format, as long as you give appropriate credit to the original author(s) and the source, provide a link to the Creative Commons licence, and indicate if you modified the licensed material. You do not have permission under this licence to share adapted material derived from this article or parts of it. The images or other third party material in this article are included in the article's Creative Commons licence, unless indicated otherwise in a credit line to the material. If material is not included in the article's Creative Commons licence and your intended use is not permitted by statutory regulation or exceeds the permitted use, you will need to obtain permission directly from the copyright holder. To view a copy of this licence, visit <http://creativecommons.org/licenses/by-nc-nd/4.0/>.

© The Author(s) 2025